Research Article

Ilham Widiyanto, Faiz Haidar Ahmad Alwan, Muhammad Arif Husni Mubarok, Aditya Rio Prabowo*, Fajar Budi Laksono, Aldias Bahatmaka, Ristiyanto Adiputra, and Dharu Feby Smaradhana

Effect of geometrical variations on the structural performance of shipping container panels: A parametric study towards a new alternative design

Abstract: In the field of logistics, containers are indispensable for shipments of large quantities of goods, particularly for exports and imports distributed by land, sea, or air. Therefore, a container must be able to withstand external loads so that goods can safely reach their destination. In this study, seven different models of container skins were developed: general honeycomb, cross honeycomb, square honeycomb, corrugated wall, flat, flat with a single stiffener, and flat with a cross stiffener. Testing was performed using the finite element method. In the static simulation, the best results were obtained by the model with corrugated walls. As the main element and the content of the sandwich panel structure, the core plays a role in increasing the ability of the structure to absorb force, thereby increasing the strength of the material. In the thermal simulation, the best results were obtained by the general honeycomb walls. Vibration simulations also showed that the square honeycomb design was better at absorbing vibration than the other models. Finally, the corrugated model had the best critical load value in the buckling simulation.

Keywords: Shipping container, finite element method, buckling analysis, thermal characteristic, vibration behavior

1 Introduction

In the field of logistics, containers are indispensable for shipments of large quantities of goods, particularly for exports and imports distributed over long distances by land, sea, or air. Containers were first used in World War II to facilitate the rapid transportation of equipment without risk to meet the needs of the war. The rapid development of technology has influenced the development of containers that are widely used by various countries to deliver shipments. A typical container on the market is illustrated in Figure 1.

Figure 1: A 20-foot shipping container

Containers that are designed as thin-walled structures [1–8] are a necessity for countries around the world that export and import products [9, 10]. Export and import programs can support a country's economy. Therefore, the choice of containers is crucial. World Bank data show that around 796 million containers were shipped be-

*Corresponding Author: Aditya Rio Prabowo: Department of Mechanical Engineering, Universitas Sebelas Maret, Surakarta 57126, Indonesia; Email: aditya@ft.uns.ac.id
Ilham Widiyanto, Faiz Haidar Ahmad Alwan, Muhammad Arif Husni Mubarok: Department of Mechanical Engineering, Universitas Sebelas Maret, Surakarta 57126, Indonesia
**Fajar Budi Laksono:** Department of Research and Development, DTECH-Engineering, Salatiga 50742, Indonesia

Aldias Bahatmaka: Interdisciplinary Program of Marine Convergence Design, Pukyong National University, Busan 48513, South Korea
**Ristiyanto Adiputra:** Department of Marine Systems Engineering, Kyushu University, Fukuoka 819-0395, Japan
Dharu Feby Smaradhana: Department of Aeronautics, Imperial College London, London SW7 2AZ, United Kingdom of Great Britain and Northern Ireland

tween 2018 and 2019, indicating their critical role in delivering shipments between countries, including those on different continents. Intercontinental distribution is supported by several large shipping logistics companies that focus on container problems. One of these shipping logistics companies has 3 million container units. Storing containers in large quantities undoubtedly requires ample space, so most shipping containers are stacked when stored, which reduces the amount of space required and thus increases the number of containers that can be accommodated. Cranes assist in stacking containers to make the transfer process easier. According to international standards, the weight of empty containers is approximately 2 tons, and the maximum weight of their contents is 22 tons. Figure 2(a) illustrates container usage for shipments from 2007 to 2017, and Figure 2(b) shows the top 10 largest container ports worldwide.
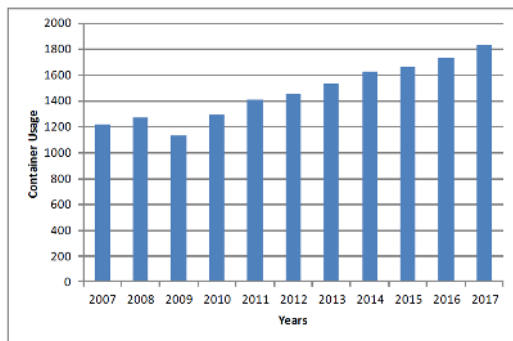
(a)
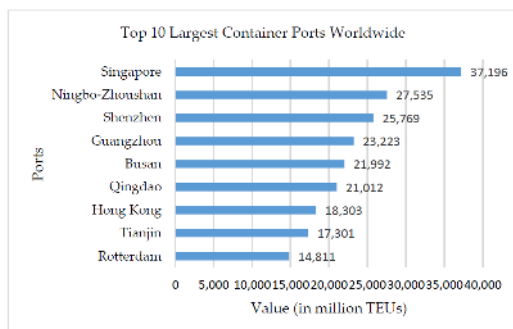
(b)

Figure 2: (a) Shipping container usage from UNCTAD [11]; (b) Top 10 largest container ports worldwide from Marine [12]

Commonly used container types are not typically resized unless they are needed for specific functions. Containers are frequently designed to have corrugated walls with contours on the inside (interior). Contours reduce the container's volume so that its internal space cannot be filled to its maximum capacity, but objects inside that hit the contour may be deformed if the impact is too hard. To save space, containers are stacked when in storage and during shipping. However, the container can become deformed if it is stacked for an extended time, especially containers toward the bottom of the stack because they bear the load of other containers. Therefore, a wall design change is necessary to resolve these issues. Conventional metal plates have been commonly used to strengthen the main structure in order to accommodate heavier loads. Metal plates are also designed to withstand vibrations during the manufacturing process and for their specific applications. Metal plates are widely used in automobile bodies, aircraft fuselages, and ship hulls due to their thin structure and light weight [13]. However, metal plates that cannot withstand high-frequency vibrations can become deformed. The shape of the plate also influences the metal's ability to withstand vibrations. Frequency values can be determined through numerical simulations in SolidWorks applications. According to Merneedi [14], the base frequency of free vibration is influenced by the number of holes and their position, which means that the frequency generated in the simulation differs between mode shapes. The modes in the simulation define the various natural frequencies that may occur, so the plate can be optimized for increased strength. Vibrations on the ship can be caused by the impact of waves hitting the ship's body [15]. Vibrations that are absorbed by one part of the ship body can be transmitted to the rest of the ship, although they are not as large as the initial vibration. Thus, containers on the ship will certainly receive vibrations, which must be absorbed mostly or entirely by the frame or body of the container.

Based on the above-described pioneer studies, improving the container design is a promising research opportunity. Therefore, the objective of this work was to explore the geometrical modification of the container panel by performing a series parametric studies using the finite element method. The structural performance of the panel was tested against several loads that are predicted to be encountered during shipping operations. The results are quantified with a focus on thermal, characteristic, vibration, and buckling behaviors.

2 Materials and methods

2.1 Design and simulation method

A standard engineering approach to structural design is to use a maximum internal stress or yield strength that is several times the safety factor of the material to prevent struc-

tural failure [13]. This method must also be sufficiently generalized to be useful in the design process. This study used the Finite Element Method (FEM) to determine the shipment container's response to static loads and to estimate the stress, strain, displacement, and safety factor. The container's frame and the wall must be strong enough to withstand shocks, heat, vibrations, and other pressures. Stress analysis using the Finite Element Method (FEM) can determine the critical point of the highest stress, as this critical value is one of the factors that can cause fatigue failure [13]. This study also realized the benefits of using CAD/CAE technology, which is frequently used for the rapid analysis of system configuration and reconfiguration of mechanical layout, electrical, and fuel systems [16]. The SolidWorks software application was used in this study. Testing can determine the actual structural mechanism, but it is very time-consuming and relatively expensive. With the development of high-performance computers and numerical methods, analysis using FEM (finite element method) can effectively and efficiently evaluate the parameters that influence the dynamic response of structures [17].

In a structural system that bears external forces, internal forces will arise on the structure's constituent elements. The internal force serves to withstand the load, which is a process that follows the law of equilibrium. If the internal force increases, then the resistance in the material increases until it reaches a maximum value. If additional load is applied beyond the maximum value, then the structural element will fail. The maximum limit of structural elements' ability to resist external loads is its strength. The structure's strength is greatly influenced by the material used, the type of loading, the structural system, temperature, the period of loading, etc.

Stress is the intensity of the internal force acting on the structural element as it resists deformation due to an external load. In general, the intensity of this force is oblique to the plane of the structure. In engineering practice, the force intensity is perpendicular and parallel to the structure being analyzed. The deformation that occurs in rod elements that receive external loads depends on the section's initial size, so it is more accurate to express it in the form of strain, which is the change in dimension per unit of measure relative to the initial dimensions [15]. Von Mises stress is a nonlinear function of the stress component. The random vibration method is commonly applied to calculate acceleration, displacement, or component stress, but it cannot be applied directly to the calculation of von Mises stress. Determining the von Mises stress from frequency requires calculating the linear stress component's length [18]. The safety factor (or factor of safety) is the ratio between the material's strength and the maxi-

mum stress of the part. If the safety factor value is greater than 1, then there is a possibility that failure will not occur. Thus, in performing the simulation, the minimum safety factor value is 1. If the safety factor value is below 1, failure will occur. If the safety factor value is close to 1 but the stress is greater than the strength, the structure cannot be designated safe. However, if the safety factor value is close to 1 but the strength is greater than the stress, then the structure can be regarded as safe.

Deformation is a change in the shape and size of an object. There are two types of deformation, namely, plastic and elastic. Plastic deformation causes an irreversible change in shape; that is, the object cannot return to its original shape. Elastic deformation is a reversible change that allows the object to return to its original shape. These changes can be caused by various factors, including force, temperature, and vibration. When deformation occurs, the object will also have various stresses and strains at each point. The extent of stress and strain can be determined by analyzing the deformation value.

Equation of Stress:

$$\sigma = \frac{F}{A} \tag{1}$$

Equation of Strain:

$$\epsilon = \frac{\Delta l}{l_0} \tag{2}$$

Equation of Displacement:

$$D = X_f - X_i \tag{3}$$

Equation of Safety Factor:

$$safety\,factor = \frac{strength}{\max stress} \tag{4}$$

Equation of Reaction Force:

$$F = -F \tag{5}$$

2.2 The effect of the sandwich construction model

Sandwich construction involves the attachment of two skins/surfaces to a core [19] and is often used in products that require certain criteria. For example, a racing car must have a low weight and fast acceleration, but it must also have high strength in case of a collision [20]. Sandwich construction is also used for airplanes, boats, shelters, skis, and other structures. A structure with this design consists of two thin plates on the outside, also called
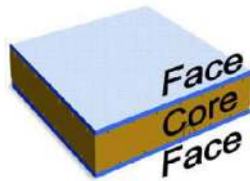
Figure 3: Illustration of the sandwich plate

a facing/skin, attached to a thick core material in the center. The surface is thin, stiff, and strong, and the core material is thicker and lighter, so the sandwich construction has low weight and high stiffness. Figure 3 shows the general structure of sandwich panels.

The purpose of attaching the skin to the core is to enable load transfer between components. The sandwich construction is similar to an "I" beam, where the sandwich's sides can be compared to the flanges in the "I" beam, and the core is analogous to a net. These sides carry the bending moment, and the other two sides are stressed. The core bears out-of-plane shear loads and separates the two surface skins. As a result, the sandwich panels have a high moment of inertia and thus high rigidity [21]. The advantage of the sandwich panel is that the entire skin area is connected to the core. Figure 4 depicts loading on sandwich panels.
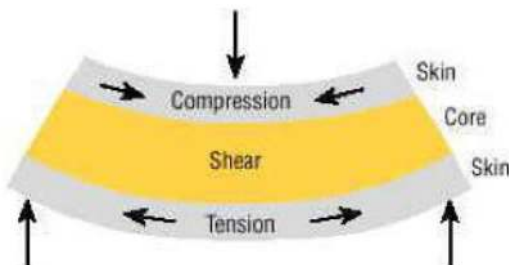

Figure 4: Plate sandwich test

2.3 Effects of using the core model

The application of a honeycomb structure helps reduce material waste, leading to reduced component weight. It also increases the specific strength with minimum material usage, which increases the capacity of the structure [22]. The honeycomb structure geometry may vary. The cells can be either column-shaped or hexagonal. In mechanical structures, the stiffness, strength, and weight efficiency are essential factors. In this research, honey-

comb, cross honeycomb, and square honeycomb models were investigated.

Yang *et al.* [23] used the finite element method in ANSYS/LS-DYNA to perform a buckling analysis on honeycomb sandwich panels of a composite shell under dynamic axial compression. Conventional methods include the honeycomb plate theory, sandwich laminboard theory, and equivalent theory. A simplified finite element model of the unit cell's hexagonal structure for sandwich panels was developed using the 3D finite element method, and the results were compared with experimental values. The yield stress calculated with finite element analysis using ANSYS/LS-DYNA had an error of 6.7% compared with the results of experiments. Structural nonlinearity was not considered because of an error. Adapa *et al.* [24] tested variations in the deformation of the honeycomb sandwich structure by performing a logical analysis, numerical model simulation, and experimental investigation using the three-point bending test. The structure consisted of a honeycomb core made of copper and stainless steel faceplates. The results of the experiment were compared with the results of the analysis; specifically, deflections for various loads and various heights of the core honeycomb structure were compared. The honeycomb core and plate skin were 2 mm thick and were connected using spot welding. It was observed that as the core height increased, the deflection in the structure decreased. Thus, increased deflection occurred at lower honeycomb core heights.

Rao *et al.* [25] conducted research on the design and analysis of aircraft lift surfaces with a honeycomb core. The maximum bending stress was applied to the upper and lower surfaces, while the center of the surface had low bending stress. Different materials were used for the honeycomb sandwich panels. A three-point bending test was conducted to understand the bending behavior of a honeycomb sandwich panel. The theoretical critical load and deflection of the honeycomb sandwich panel were calculated, and the three-point bending test revealed that the titanium alloy had the greatest strength-to-weight ratio. A crushing test was also carried out by varying the cell thickness and honeycomb core height. The results of the crushing test showed that the thickness of the honeycomb core cell wall was a critical variable that affected the crushing strength of the sandwich panel under lateral crushing loads, and the honeycomb core height did not influence the crushing behavior. Jangavali *et al.* [26] performed a three-point bending and impact test on a honeycomb panel. Aluminum material was used as the core with an FRP face sheet in the honeycomb panel. ANSYS was also used for the finite element analysis of honeycomb panels. The theoretical critical load was determined and com-

pared with the experimental and FEA results. Deformation was determined from the impact test and compared with the results of the FEA. The critical load was found to vary by 5-6% between the experimental and FEA results. The deformations determined experimentally were slightly larger than those calculated in the FEA.

Wang *et al.* [27] conducted a quasi-static theoretical model test. In their research, they were able to effectively predict the average force of a hexagonal tube at axial pressure. The analytical solutions closely matched the numerical results, and they revealed the mechanism by which each criterion significantly increased in the simulation using the mechanical theory. This shows that a reinforcement design can reuse internal space to some extent and can substantially increase the tubes' energy absorption capability. Thin-walled models are widely used in automobile bodies, aircraft fuselages, and ship hulls because they are thin and lightweight [28]. One of the models commonly used in containers is corrugated. The corrugated model is used because it has a thin shape but can absorb a greater force than ordinary plates [28, 29]. However, corrugated walls introduce difficulties in the fabrication or manufacturing process of such structures [29]. In his research, Abramowicz [30] stated that the corrugated form could receive a more significant impact than ordinary plates. The increase in energy absorption is proportional to the additional weight of the model. Corrugated walls will be slightly heavier than a plate, but the absorbance capacity will also increase. Figure 5 shows the detailed geometric description of the honeycomb.
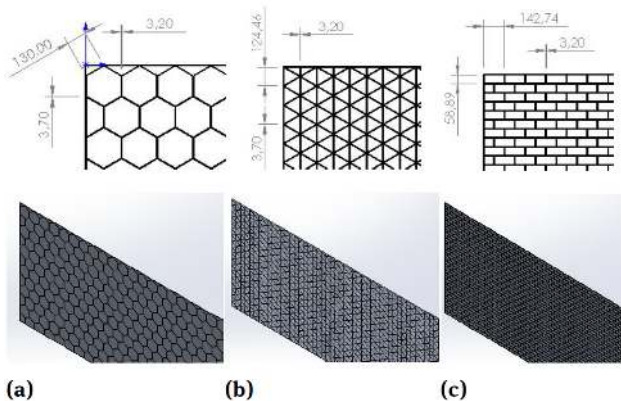

Figure 5: Geometrical models of the modified container panel: (a) general honeycomb, (b) cross honeycomb, and (c) square honeycomb

Ha and Lu [29] examined the characteristics of the corrugated design and measured its deformation during energy absorption. The corrugated wall is generally used in the bodies of containers because it is light but can absorb external forces from the container. Metal plates are widely used to increase structural strength due to their superior strength, high initial stiffness, and excellent ductility [31]. Clayton *et al.* [32] examined the characteristics and performance of corrugated panels and found significant ductility and energy dissipation. Figure shows the detailed geometric description of the corrugated wall.
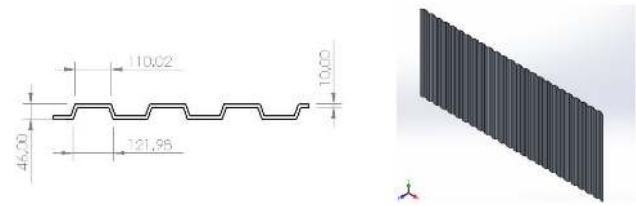

Figure 6: Geometrical model of the corrugated wall

The strength of the corrugated plate was compared with that of the flat plate by Emami *et al.* [33] and Qiu *et al.* [34]. Their research shows that the ultimate strength value of the corrugated plate is lower than that of the flat plate. However, the stiffness, elasticity, and energy absorption values of the corrugated plate are significantly better than those of the flat plate. For this reason, many designers choose to use corrugated plates instead of flat plates. Although the corrugated plate is slightly heavier than the flat plate, due to its characteristics, the corrugated plate is the stronger of the two. Figure 8 shows the detailed geometric description of the flat wall with a single stiffener, while Figure 9 shows the detailed geometric description of the flat wall with a cross stiffener.
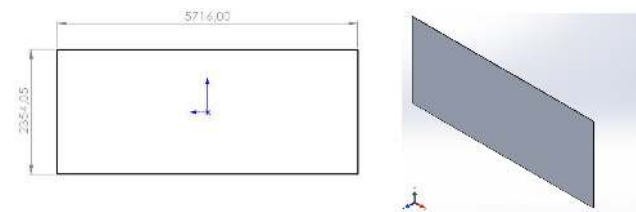

Figure 7: Geometrical model of the flat wall

2.4 Material properties

Most containers are made of aluminium because it is lighter than steel, and in a refrigerated container, a thick insulating layer must be used to maintain the internal temperature [22, 23]. Aluminium is a material that is character-
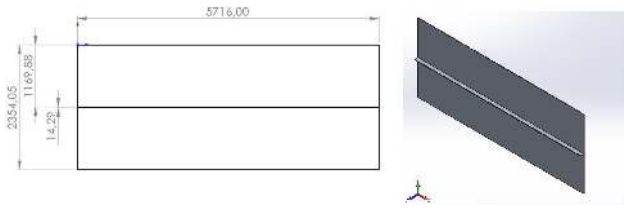
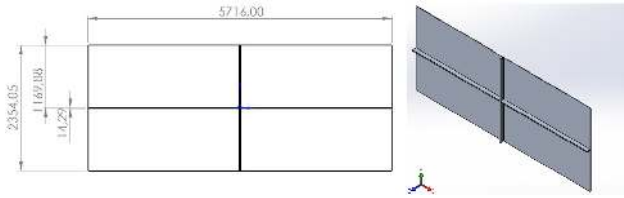**Figure 8:** Geometrical model of the flat wall with a single stiffener

Figure 9: Geometrical model of the flat wall with a cross stiffener

ized by a light weight, low density, high specific strength, and high stiffness. It is widely applied in automobile, aviation, aerospace, and other industries that require a light structure [35, 36]. Aluminium can also minimize air leakage and has the advantage of thermal efficiency. All of the walls of these containers are made according to ISO standards. In this study, the designed and analyzed structures were made from aluminium 6061-O. The material was applied to the product and simulated according to its expected use, and the models were compared. The material properties of aluminium 6061-O are listed in Table 1.

Table 1: Material properties of aluminium 6061-O

Mechanical properties	Value and unit
Density	2.70E+03 kg/m^3
Poisson's ratio	3.30E−01
Shear modulus	2.6E+10 N/m^2
Tensile strength	1.25E+08 N/m^2
Yield strength	6.21E+07 N/m^2
Thermal expansion coefficient	2.4E−05 /K
Thermal conductivity	1.80E+02 W/(m·K)
Specific heat	8.96E+02 J/(kg·K)

2.5 Thermal analysis

Thermal analysis involves different techniques to analyze the time and temperature at which physical changes occur when a substance is heated or cooled [37]. Each technique is defined according to the type of physical change being analyzed. When evaluating a material's characteristics,

it is necessary to use different techniques or a combination of several techniques depending on the purpose. The study of temperature gradients is essential for industries that require the refrigeration of rooms and containers. In this study, seven different models were simulated: general honeycomb, cross honeycomb, square honeycomb, corrugated wall, flat wall, flat with a single stiffener, and flat with a cross stiffener. The material is aluminium 6061-O, and the convection coefficient of each object is in Table 2.

Table 2: List of the convection coefficients of all studied models

Model	Convection coefficient (W/(m^2·K))
General honeycomb	15.17
Cross honeycomb	15.17
Square honeycomb	15.17
Corrugated wall	27.23
Flat wall	24.865
Flat with single stiffener	24.865
Flat with cross stiffener	24.865

This simulation assumed that the temperature is 40°C on the outside surface and 30°C on the inside surface. In this study, we assumed that heat transfer in the container shells occurs by convection because the heat from the outside will pass through the air to the container's surface. The convection coefficient depends on the thickness of the model. The bulk ambient temperature was assumed to be 308 Kelvin or 35°C. Equations 6–9 define the convection heat transfer formula used in the analysis.

$$q_h = hA(T_s - T_f) \tag{6}$$

Reynolds Number Equation:

$$Re = \frac{V.L}{v} \tag{7}$$

Nusselt Number Equation:

$$Nu = \frac{h.L}{k} = 0.04Re^{0.85}Pr^{1/3} \tag{8}$$

Convection Coefficient Equation:

$$h = \frac{Nu.k}{L} \tag{9}$$

2.6 Vibration analysis

The simulations in this work included static and vibration analyses (modal analysis is often involved for shell-based

structures [38–45]). The static simulation was carried out to determine the effect of stacking containers. The load applied to the container was 20,000 N, and the simulations were performed assuming the weight of an empty container. The simulation was performed to evaluate the stress, displacement, strain, and safety factor values. Vibration needs to be simulated because the ship will undoubtedly experience vibrations when it is hit by waves in the ocean. A container that receives vibrations may be deformed, which can cause the container stack to slip and even fall [46]. Therefore, the aim of this simulation was to quantify the behavior of a container subjected to a defined vibration profile. SolidWorks was used to evaluate a container structure that is strong and able to withstand the given load. Equations for force and plate motion without a load are as follows:

$$D\nabla^2\nabla^2 w\left(x, y, t\right) = p\left(x, y, t\right) - \rho h \frac{\partial^2 w}{\partial t^2}(x, y, t) \qquad (10)$$

where p and w are functions of time, ρ is the density of the material, and h is the thickness of the plate. The vibration $p(x, y, t)$ causes a dynamic response:

$$\omega_0 = \omega\sqrt{\frac{\rho h a^4}{D}} \qquad (11)$$

Equation (11) is the natural frequency of a square plate. $D = \frac{Eh^3}{12(1-\vartheta^2)}$, h = thickness of the plate, ρ = density, ϑ = Poisson's ratio, and E = Young's modulus. Seven variations were simulated: corrugated, honeycomb, cross honeycomb, square honeycomb, one stiffener, cross stiffener, and flat. We aimed to determine which of these seven models had the best strength-to-weight ratio, as containers that are too heavy will reduce efficiency when they are loaded onto the ship.

2.7 Buckling analysis

Buckling occurs when a structure is unable to maintain its original shape. The consequence of buckling is a fundamental geometric problem, where there is a large deflection that changes the shape of the structure [47]. Buckling is an instability phenomenon that usually occurs in thin rods, plates, and shells (in this case, the container wall).

Buckling simulations are performed to calculate the critical buckling load that causes unstable conditions and the buckling mode shape, which defines the shape characteristics related to the response of structures that experience buckling [48]. The buckling load or critical buckling load is the load at which the current equilibrium state of an element or structure suddenly changes to become unstable or to another stable configuration with or without a significant response (deformation or deflection). Thus, the bending load is the most significant load whose equilibrium stability exists on a structural element or structure in its original (or previous) equilibrium configuration. Buckling needs to be simulated because the containers bear loads when stacked. When receiving pile loads, containers may be deformed so that the stack of containers buckles. Therefore, this simulation aimed to identify the container skin with the highest safety factor.

Equation of Safety Factor:

$$safety\ factor = \frac{strength}{\max stress} \qquad (12)$$

The critical buckling load can be calculated using Euler's formula:

$$P_{cr} = \frac{\pi^2.El}{L^2} \qquad (13)$$

Regardless of the final condition, the critical load does not depend on the material's strength but rather depends on the bending stiffness. The bending resistance can be increased by increasing the moment of inertia. This simula-
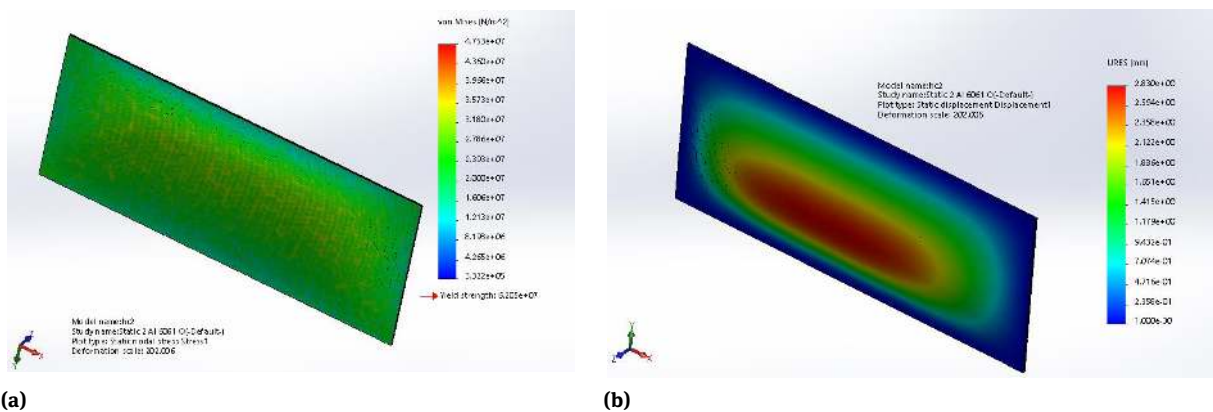

(a)

(b)

Figure 10: Results for the general honeycomb: (a) Von Mises stress and (b) resultant displacement
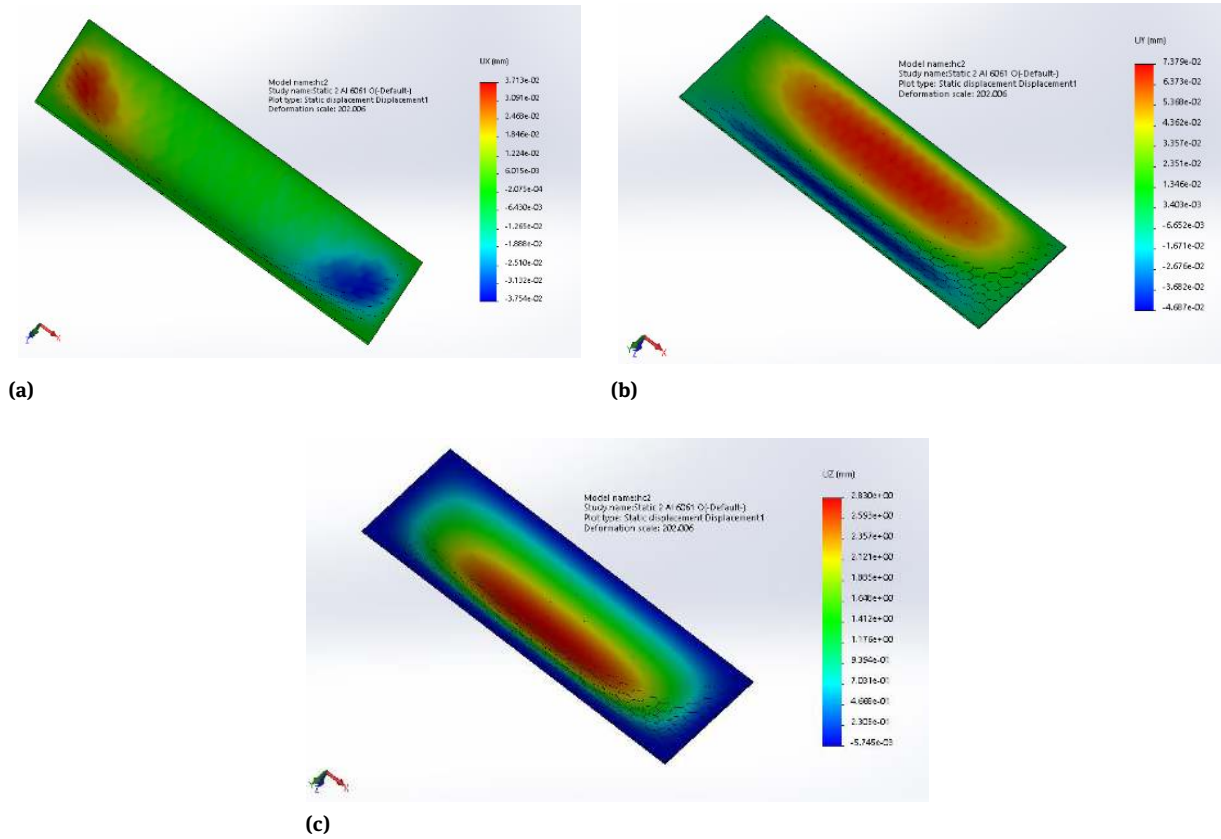
(a)

(b)

(c)

Figure 11: Displacement of the general honeycomb: (a) x-axis, (b) y-axis, (c) z-axis
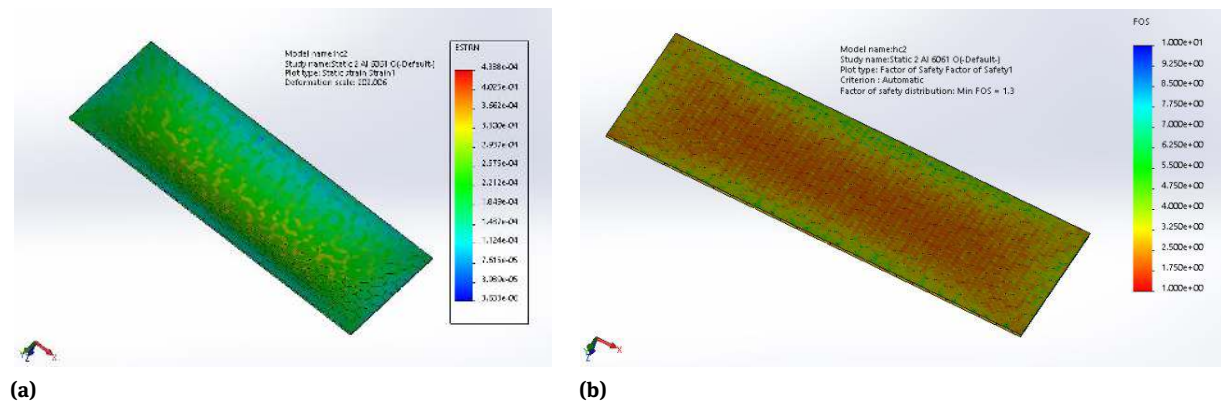

(a)

(b)

Figure 12: Results for the general honeycomb: (a) Strain and (b) safety factor

tion evaluated seven different models: honeycomb, cross honeycomb, square honeycomb, corrugated, flat, flat with a single stiffener, and flat with a cross stiffener. The material used is aluminium 6061-O. This simulation was carried out using a critical load input to obtain a minimum safety factor value of 1, the threshold for failure.

3 Calculation results

3.1 Static analysis based on thermal loading

3.1.1 General honeycomb

Figure 10 shows the static simulation results using aluminium 6061-O as the material. In the static simulation, the lowest value of von Mises stress is 3.32E+02 N/mm^2,

and the highest value is 4.75E+04 N/mm^2 (Figure 10a). Figure 10b shows that the highest value obtained for the resultant displacement is 2.83E+03 mm. Figure 11 shows the static simulation results for aluminium 6061-O on the x-, y-, and z-axes. In the static simulation, the displacement of each axis is 2.36E−02 mm, 4.67E−02 mm, and 1.79E+00 mm.

The results in Figure 12a show that the lowest value of strain is 2.72E−03, and the highest value is 2.80E−01. Furthermore, Figure 12b indicates that the lowest value of the safety factor is 2.38E+03, and the highest value is 3.09E+05.

3.1.2 Cross honeycomb

The static simulation of the cross honeycomb indicates that the lowest value of von Mises stress is 1.65E+02 N/mm^2, and the highest value is 7.97E+04 N/mm^2 (Figure 13a). Figure 13b shows that the highest value of the resultant displacement is 2.78E+03 mm.

Figure 14 shows the static simulation results for aluminium 6061-O on the x-, y-, and z-axes. The displacement

of each axis is 3.96E−02 mm, 6.24E−02 mm, and 2.78E+00 mm. Figure 15a indicates that the lowest value of strain is 2.79E−03, and the highest value is 6.02E−01. Figure 15b reveals that the lowest value of the safety factor is 7.79E+02, and the highest value is 3.77E+05.

3.1.3 Square honeycomb

Figure 16a shows that the lowest value of von Mises stress is 1.31E+02 N/mm^2, and the highest value is 8.34E+04

(a)

(a)

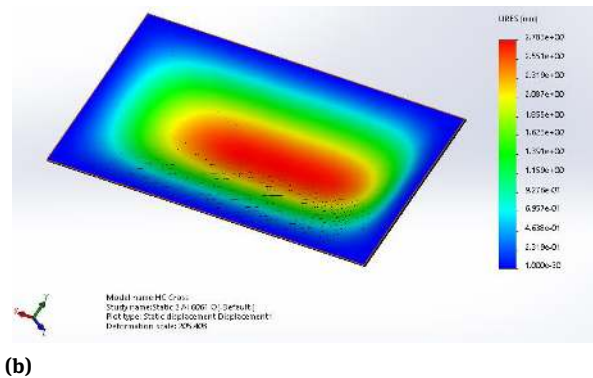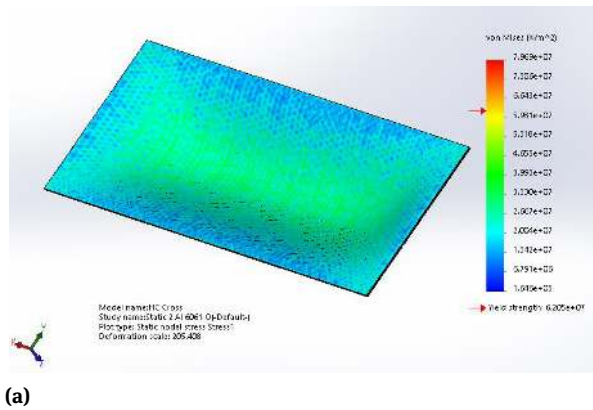**(b)**

(b)

(c)

Figure 13: Results for the cross honeycomb: (a) Von Mises stress and (b) resultant displacement
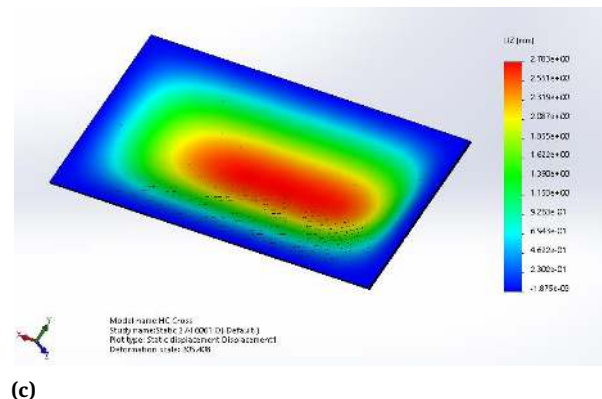
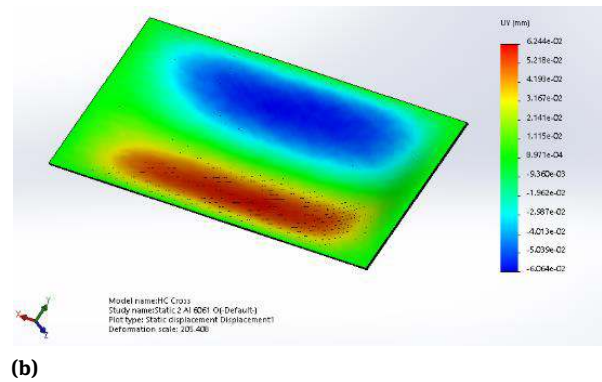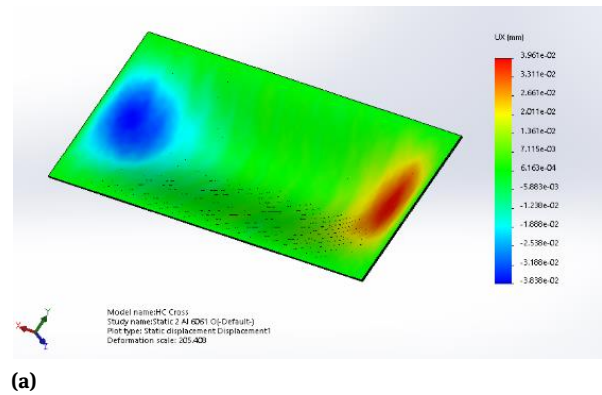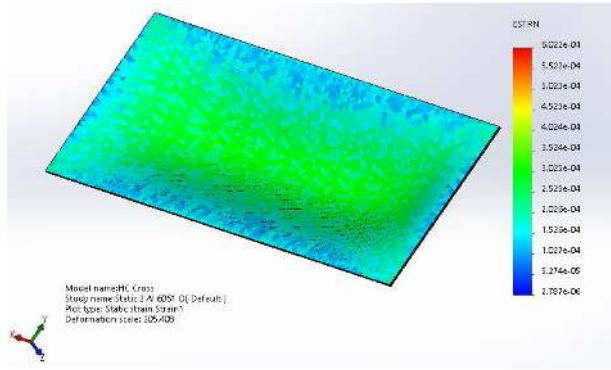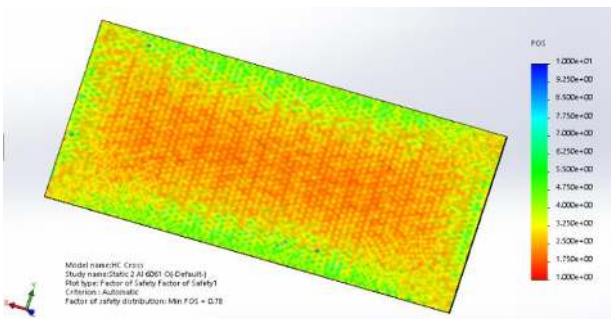**Figure 14:** Displacement of the cross honeycomb in the static simulation: (a) x-axis, (b) y-axis, and (c) z-axis
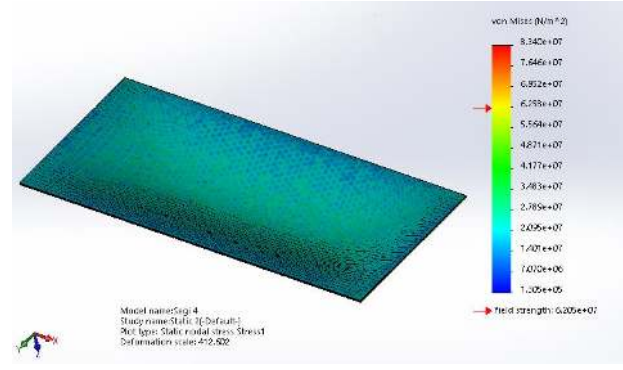
(a)

(b)

Figure 15: Results for the cross honeycomb: (a) strain and (b) safety factor

(a)

(b)

Figure 16: Results for the square honeycomb: (a) Von Mises stress and (b) resultant displacement

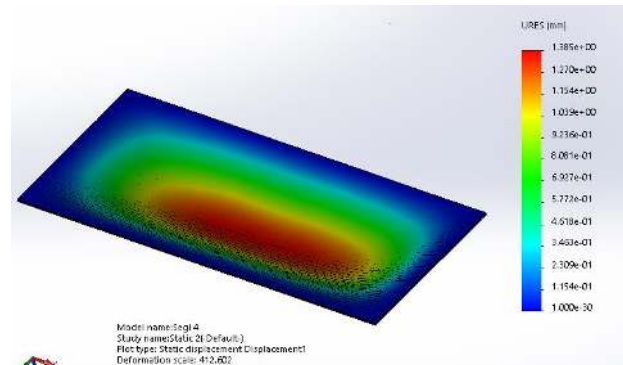N/mm^2. The highest value of the resultant displacement is 1.39E+03 mm, as shown in Figure 16b.

Figure 17 shows the static displacement results for aluminium 6061-O on the x-, y-, and z-axes. The displacement of each axis is 2.00E–02 mm, 3.05E–02 mm, and 1.39E+00 mm. Figure 18a displays the lowest value of strain, which is 1.17E–03, while the highest value is 4.06E–01. The lowest value of the safety factor is 7.44E+02, and the highest value is 4.75E+05 (see Figure 18b).

3.1.4 Summary of overall static analyses: thermal loading

In addition to the difference in results between general, cross, and square honeycombs, static analysis based on thermal loadings also varied depending on the applied materials. The overall results for the von Mises stress and reaction force for all the applied materials and designed geometries are presented in Table 3, while the displacement results are shown in Table 4. The summarized strain results are in Table 5, and the safety factor results are provided in Table 6. Tables 3–6 show the statistical results,

which show that the von Mises stress is the criterion least affected by the thermal load, with a coefficient of variance of 7.34E–01%. The maximum reaction force value is the criterion most influenced by the thermal load, with a variance coefficient of 4.47E+00%. The maximum stress is the criterion most influenced by the thermal load, with a standard deviation of 2.79E+10. The minimum strain is the criterion least affected by the thermal load, with a standard deviation of 8.42E–03.

3.1.5 Summary of overall static analyses: buckling condition

A static analysis was also conducted using the configuration applied in the buckling assessment. The statistical results in Tables 7–9 reveal that the maximum strain is the criterion least affected by the buckling factor of safety, with a coefficient of variance of 1.00E+00%. Additionally, the maximum stress is the criterion most influenced by the safety factor, with a variance coefficient of 1.31E+16%. The maximum stress is the criterion most influenced by
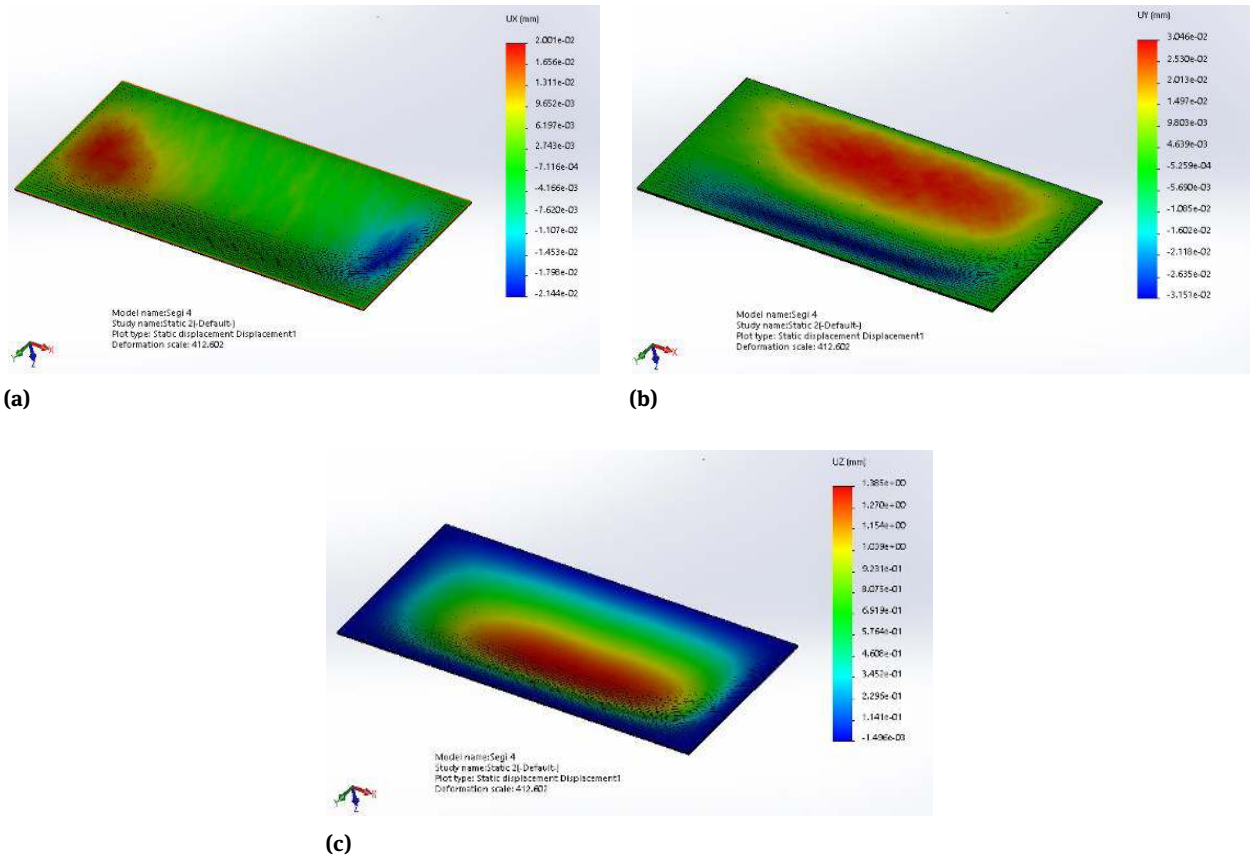
Figure 17: Displacement of the square honeycomb in the static simulation: (a) x-axis, (b) y-axis, (c) z-axis
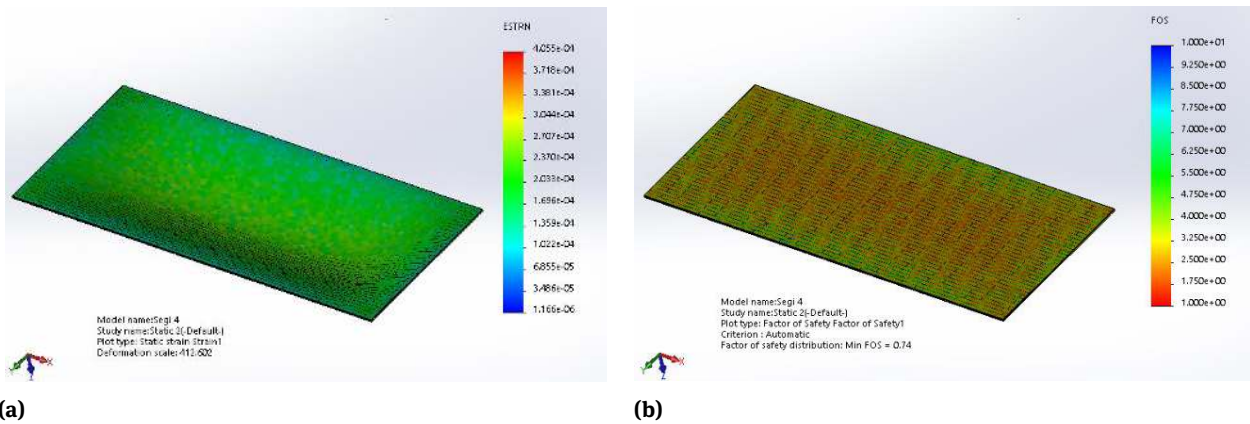
Figure 18: Results for the square honeycomb: (a) Strain and (b) safety factor

the safety factor, with a standard deviation of 1.14E+08. Finally, the minimum strain is the criterion least affected by the safety factor, with a standard deviation of 6.82E−04.

3.2 Thermal analysis

3.2.1 General honeycomb

Figure 19 shows the thermal simulation results for the outer surface, inner surface, and edge of the panel, with aluminium 6061-O as the material. In the thermal simula-

Table 3: Summary of the von Mises stress and reaction force results

Model	Material	Reaction Force (N)	Von Mises stress (N/mm^2)	
			min	max
General honeycomb	A304	1.31E+11	6.70E+02	8.70E+04
	6061-O	7.85E+05	3.32E+02	4.75E+04
	7075 T6	8.05E+05	3.41E+02	4.88E+04
Honeycomb cross	A304	1.89E+05	3.47E+02	1.36E+05
	6061-O	1.12E+05	1.65E+02	7.97E+04
	7075 T6	1.15E+05	1.69E+02	8.18E+04
Square honeycomb	A304	9.56E+04	1.82E+02	1.50E+05
	6061-O	5.65E+04	1.31E+02	8.34E+04
	7075 T6	5.80E+04	1.34E+02	8.56E+04
Corrugated	A304	1.84E+05	1.03E+03	7.32E+04
	6061-O	1.10E+05	5.17E+02	3.99E+04
	7075 T6	1.13E+05	5.30E+02	4.10E+04
Flat	A304	4.28E+04	1.15E−04	8.53E+04
	6061-O	2.53E+04	6.44E−05	4.55E+04
	7075 T6	2.59E+04	8.49E−03	4.67E+04
Flat with single stiffener	A304	1.93E+05	1.39E+03	3.85E+05
	6061-O	1.14E+05	9.94E+02	2.23E+05
	7075 T6	1.17E+05	1.02E+03	2.29E+05
Flat with cross stiffener	A304	2.65E+05	1.29E+03	1.90E+05
	6061-O	1.15E+05	1.17E−02	8.64E+04
	7075 T6	1.62E+05	5.17E+02	1.11E+05
Mean		6.25E+09	4.65E+02	1.12E+05
Median		1.15E+05	3.41E+02	8.53E+04
Sample variance		7.81E+20	1.85E+05	6.79E+09
Standard deviation		2.79E+10	4.30E+02	8.24E+04
Variance coeff. (%)		4.47E+00	9.26E−01	7.34E−01
Standard error		6.10E+09	9.38E+01	1.80E+04

Table 4: Summary of the displacement results

Model	Material	Displacement (mm)			
		Resultant	X	Y	Z
General honeycomb	A304	1.79E+03	2.36E−02	4.67E−02	1.79E+00
	6061-O	2.83E+03	3.71E−02	7.74E−02	2.83E+00
	7075 T6	2.78E+03	3.65E−02	7.26E−02	2.78E+00
Honeycomb cross	A304	1.77E+03	2.54E−02	4.02E−02	1.77E+00
	6061-O	2.78E+03	3.96E−02	6.24E−02	2.78E+00
	7075 T6	2.74E+03	3.90E−02	6.14E−02	2.74E+00
Square honeycomb	A304	8.90E+02	1.28E−02	1.98E−02	8.90E−01
	6061-O	1.39E+03	2.00E−02	3.05E−02	1.39E+00
	7075 T6	1.36E+03	1.97E−02	3.00E−02	1.36E+00
Corrugated	A304	1.78E+03	9.33E−02	9.59E−03	5.39E−02
	6061-O	2.91E+03	1.50E−01	1.29E−02	8.77E−02
	7075 T6	2.86E+03	1.47E−01	1.27E−02	8.62E−02
Flat	A304	5.83E+03	3.61E−02	4.78E−02	2.74E−03
	6061-O	8.94E+03	5.60E−02	7.34E−02	4.13E−03
	7075 T6	8.79E+03	5.50E−02	7.21E−02	4.06E−03
Flat with single stiffener	A304	1.73E+04	1.05E+00	1.47E−01	1.68E−03
	6061-O	2.74E+04	1.66E+00	2.33E−01	2.42E−03
	7075 T6	2.69E+04	1.64E+00	2.30E−01	2.38E−03
Flat with cross stiffener	A304	4.31E+03	2.78E−01	2.49E−01	1.82E−03
	6061-O	4.95E+03	3.12E−01	2.85E−01	6.25E−03
	7075 T6	6.83E+03	4.47E−01	4.00E−01	2.61E−03
Mean		6.53E+03	2.94E−01	1.05E−01	8.85E−01
Median		2.86E+03	5.50E−02	6.24E−02	8.62E−02
Sample variance		5.81E+07	2.46E−01	1.13E−02	1.21E+00
Standard deviation		7.62E+03	4.96E−01	1.06E−01	1.10E+00
Variance coeff. (%)		1.17E+00	1.69E+00	1.01E+00	1.24E+00
Standard error		1.66E+03	1.08E−01	2.32E−02	2.40E−01

Table 5: Summary of the strain results

Model	Material	Strain (-)	
		min	max
General honeycomb	A304	2.72E−03	2.80E−01
	6061-O	3.63E−03	4.39E−01
	7075 T6	3.57E−03	4.31E−01
Honeycomb cross	A304	1.49E−03	3.58E−01
	6061-O	2.79E−03	6.02E−01
	7075 T6	2.74E−03	5.92E−01
Square honeycomb	A304	1.19E−03	2.58E−01
	6061-O	1.17E−03	4.06E−01
	7075 T6	1.15E−03	3.99E−01
Corrugated	A304	2.84E−03	2.38E−01
	6061-O	7.17E−03	3.75E−01
	7075 T6	7.05E−03	3.69E−01
Flat	A304	1.10E−02	2.78E−01
	6061-O	1.68E−02	4.26E−01
	7075 T6	1.65E−02	4.19E−01
Flat with single stiffener	A304	1.44E−02	1.58E+00
	6061-O	2.10E−02	2.63E+00
	7075 T6	2.06E−02	2.59E+00
Flat with cross stiffener	A304	2.08E−02	7.22E−01
	6061-O	2.43E−02	8.81E−01
	7075 T6	2.46E−02	1.15E+00
Mean		9.88E−03	7.34E−01
Median		7.05E−03	4.26E−01
Sample variance		7.10E−05	4.70E−01
Standard deviation		8.42E−03	6.86E−01
Variance coeff. (%)		8.53E−01	9.34E−01
Standard error		1.84E−03	1.50E−01

Table 6: Summary of the safety factor results

Model	Material	Safety Factor (-)
General Honeycomb	A304	2.38E+03
	6061-O	1.31E+03
	7075 T6	1.04E+04
Honeycomb Cross	A304	1.52E+03
	6061-O	7.79E+02
	7075 T6	6.18E+03
Square honeycomb	A304	1.38E+03
	6061-O	7.44E+02
	7075 T6	5.90E+03
Corrugated	A304	2.83E+03
	6061-O	1.55E+03
	7075 T6	1.23E+04
Flat	A304	2.42E+00
	6061-O	1.36E+00
	7075 T6	1.08E+01
Flat with single stiffener	A304	5.38E+02
	6061-O	2.78E+02
	7075 T6	2.20E+03
Flat with cross stiffener	A304	1.09E+03
	6061-O	7.18E+02
	7075 T6	4.56E+03
Mean		2.70E+03
Median		1.38E+03
Sample variance		1.10E+07
Standard deviation		3.31E+03
Variance coeff. (%)		1.23E+00
Standard error		7.22E+02

Table 7: Summary of the critical load and von Mises stress results

Model	Material	Critical Load (N)	Stress (N/mm^2)	
			Min	Max
General honeycomb	A304	1.18E+07	3.95E+00	2.06E+02
	6061O	3.37E+06	8.46E−01	6.21E+01
	7075 T6	2.70E+07	6.79E+00	4.98E+02
Cross honeycomb	A304	8.50E+06	1.64E+00	2.06E+02
	6061O	2.70E+06	5.88E−01	6.22E+01
	7075 T6	2.20E+07	4.74E+00	5.07E+02
Square honeycomb	A304	1.20E+07	1.56E+06	2.08E+08
	6061O	3.40E+06	4.40E+05	6.22E+07
	7075 T6	2.77E+07	3.56E+06	5.07E+08
Corrugated	A304	1.16E+07	8.01E+01	2.07E+02
	6061O	3.37E+06	1.91E+01	6.20E+01
	7075 T6	2.70E+07	1.53E+02	4.97E+02
Flat	A304	5.87E+06	4.66E+01	2.07E+02
	6061O	1.60E+06	1.09E+01	6.03E+01
	7075 T6	1.30E+07	8.85E+01	4.90E+02
Flat with single stiffener	A304	6.90E+06	1.94E−01	2.07E+02
	6061O	1.96E+06	6.63E−02	6.19E+01
	7075 T6	1.60E+07	5.41E−01	5.05E+02
Flat with cross stiffener	A304	7.13E+06	1.07E−01	2.06E+02
	6061O	2.00E+06	3.31E−02	6.15E+01
	7075 T6	3.10E+06	5.13E−02	9.53E+01
Mean		1.04E+07	2.65E+05	3.70E+07
Median		7.13E+06	4.74E+00	2.07E+02
Sample variance		1.93E+06	1.81E+05	2.56E+07
Standard deviation		8.61E+06	8.11E+05	1.14E+08
Variance coeff. (%)		7.41E+13	6.58E+11	1.31E+16
Standard error		8.29E−01	3.06E+00	3.09E+00

Table 8: Summary of the displacement results

Model	Material	Displacement (mm)			
		Resultant	X	Y	Z
General honeycomb	A304	1.38E+00	4.30E−01	1.32E+00	1.16E−02
	6061O	1.10E+00	3.85E−01	1.04E+00	1.02E−02
	7075 T6	8.47E+00	2.96E+00	7.97E+00	7.83E−02
Cross honeycomb	A304	9.91E−01	3.16E−01	9.42E−01	1.12E−02
	6061O	8.83E−01	3.15E−01	8.25E−01	9.50E−03
	7075 T6	6.89E+00	2.46E+00	6.44E+00	7.42E−02
Square honeycomb	A304	1.41E+00	4.39E−01	1.34E+00	1.70E−02
	6061O	1.12E+00	3.91E−01	1.04E+00	1.46E−02
	7075 T6	8.71E+00	3.06E+00	8.16E+00	1.15E−01
Corrugated	A304	2.14E+00	2.81E−01	1.95E−01	2.11E+00
	6061O	1.71E+00	2.58E−01	1.72E−01	1.68E+00
	7075 T6	1.32E+01	1.98E+00	1.32E+00	1.29E+01
Flat	A304	1.18E+00	3.79E−01	1.12E+00	2.48E−02
	6061O	9.02E−01	3.25E−01	8.42E−01	2.12E−02
	7075 T6	7.03E+00	2.53E+00	6.55E+00	1.65E−01
Flat with single stiffener	A304	3.60E+00	4.61E−01	1.32E+00	3.40E+00
	6061O	3.13E+00	4.12E−01	1.03E+00	2.99E+00
	7075 T6	2.45E+01	3.22E+00	8.09E+00	2.34E+01
Flat with cross stiffener	A304	5.69E+00	4.50E−01	1.30E+00	5.52E+00
	6061O	5.17E+00	3.98E+00	1.01E+00	5.05E+00
	7075 T6	7.67E+00	5.90E−01	1.49E+00	7.51E+00
Mean		5.09E+00	1.05E+00	2.55E+00	3.10E+00
Median		3.13E+00	4.30E−01	1.30E+00	1.15E−01
Sample variance		3.01E+01	1.15E+00	7.73E+00	3.11E+01
Standard deviation		5.48E+00	1.07E+00	2.78E+00	5.58E+00
Variance coeff. (%)		1.08E+00	1.02E+00	1.09E+00	1.80E+00
Standard error		1.23E+00	2.40E−01	6.22E−01	1.25E+00

Table 9: Summary of the strain results

| Model	Material	Strain (-)	
		Min	**Max**
General honeycomb	A304	1.35E−05	9.51E−04
	6061O	1.49E−05	8.21E−04
	7075 T6	1.14E−04	6.31E−03
Cross honeycomb	A304	1.58E−05	7.64E−04
	6061O	1.32E−05	7.58E−04
	7075 T6	1.04E−04	5.92E−03
Square honeycomb	A304	1.74E−05	9.38E−04
	6061O	2.08E−05	7.99E−04
	7075 T6	1.63E−04	6.25E−03
Corrugated	A304	5.21E−04	8.78E−04
	6061O	3.95E−04	7.38E−04
	7075 T6	3.04E−03	5.67E−03
Flat	A304	2.46E−04	8.46E−04
	6061O	1.73E−04	7.09E−04
	7075 T6	1.35E−03	5.52E−03
Flat with single stiffener	A304	3.09E−07	9.32E−04
	6061O	2.68E−07	8.00E−04
	7075 T6	2.10E−06	6.26E−03
Flat with cross stiffener	A304	1.05E−06	9.21E−04
	6061O	1.09E−06	7.81E−04
	7075 T6	1.63E−06	1.16E−03
Mean		2.95E−04	2.32E−03
Median		1.74E−05	9.21E−04
Sample variance		4.66E−07	5.42E−06
Standard deviation		6.82E−04	2.33E−03
Variance coeff. (%)		2.31E+00	1.00E+00
Standard error		1.53E−04	5.21E−04

(a)

(b)

(c)
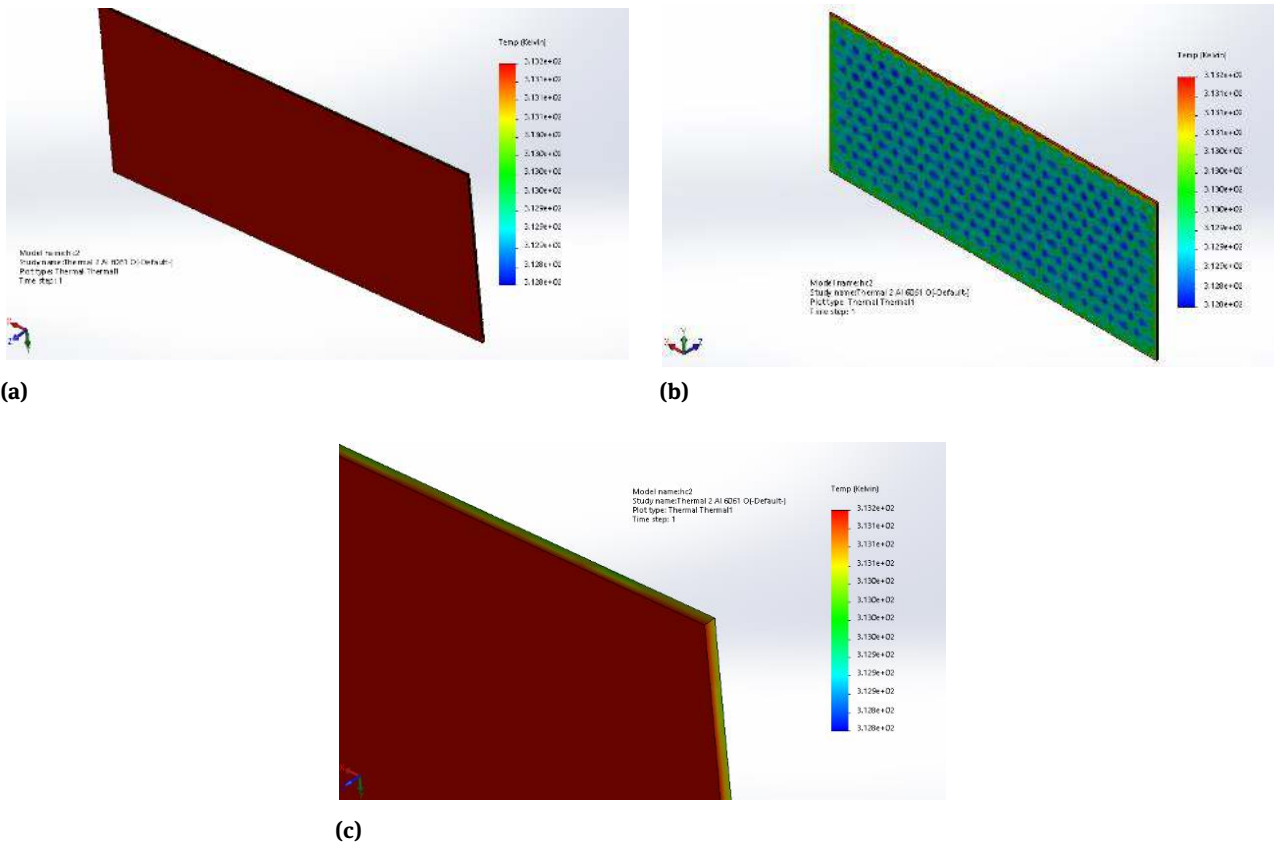
Figure 19: Result of the thermal simulation for the general honeycomb: (a) outer surface, (b) inner surface, and (c) edge
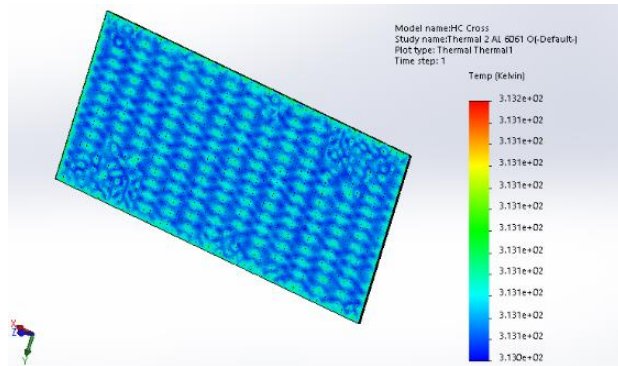
tion, the lowest value is 3.13E+05 Kelvin, and the highest value is 3.13E+05 Kelvin.
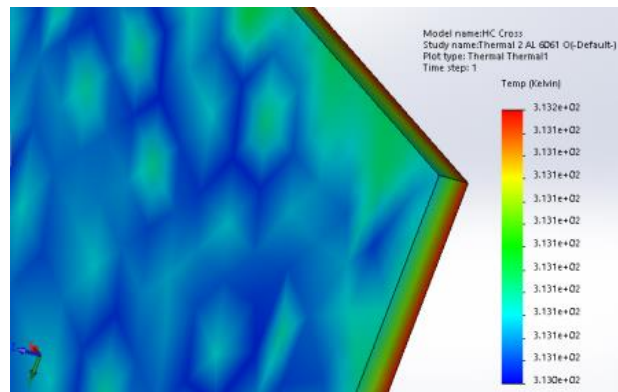
3.2.2 Cross honeycomb

Figure 20 shows the thermal simulation results for the outer surface, inner surface, and edge of the panel, with
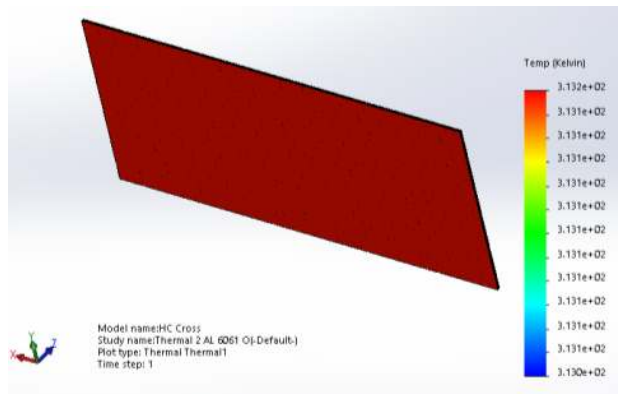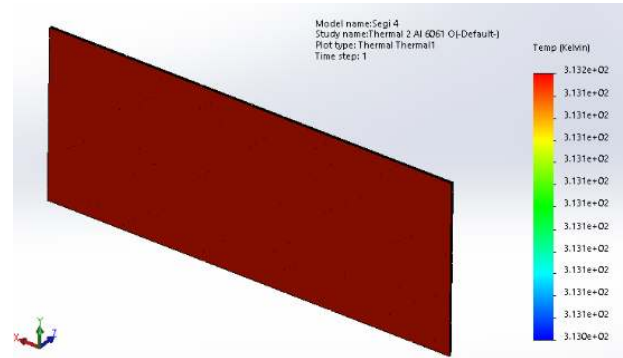

(a)

(b)

(c)

Figure 20: Result of the thermal simulation for the cross honeycomb: (a) outer surface, (b) inner surface, (c) edge
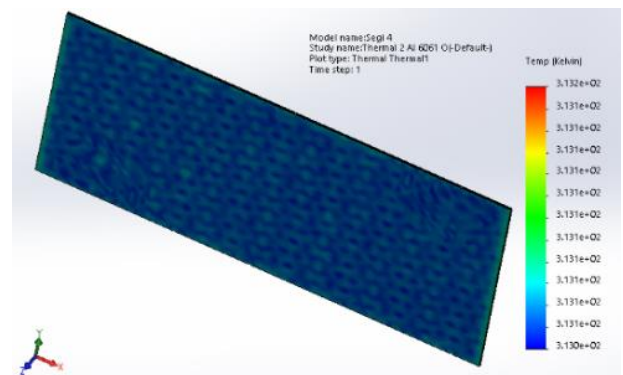
aluminium 6061-O as the material. In the thermal simulation, the lowest value is 3.13E+05 Kelvin, and the highest value is 3.13E+05 Kelvin.
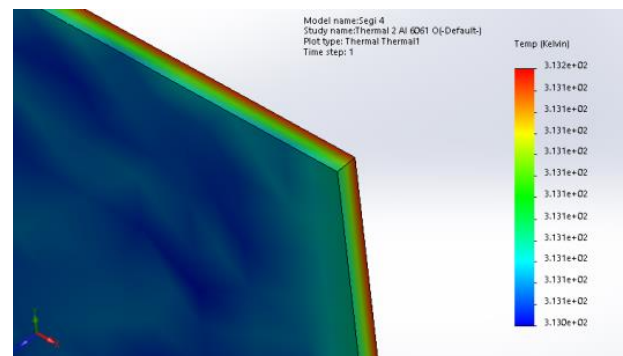
3.2.3 Square honeycomb

Figure 21 shows the thermal simulation results for the outer surface, inner surface, and edge of the panel, with aluminium 6061-O as the material. In the thermal simula-

(a)

(b)

(c)

Figure 21: Result of the thermal simulation for the square honeycomb: (a) outer surface, (b) inner surface, (c) edge

tion, the lowest value is 3.13E+05 Kelvin, and the highest value is 3.13E+05 Kelvin.

tion, the lowest value is 3.13E+05 Kelvin, and the highest value is 3.13E+05 Kelvin.

3.2.4 Corrugated wall

Figure 22 shows the thermal simulation results for the outer surface, inner surface, and edge of the panel, with aluminium 6061-O as the material. In the thermal simula-

3.2.5 Flat wall

Figure 23 shows the thermal simulation results for the outer surface, inner surface, and edge of the panel, with aluminium 6061-O as the material. In the thermal simulation, the lowest value is 3.13E+05 Kelvin, and the highest value is 3.13E+05 Kelvin.
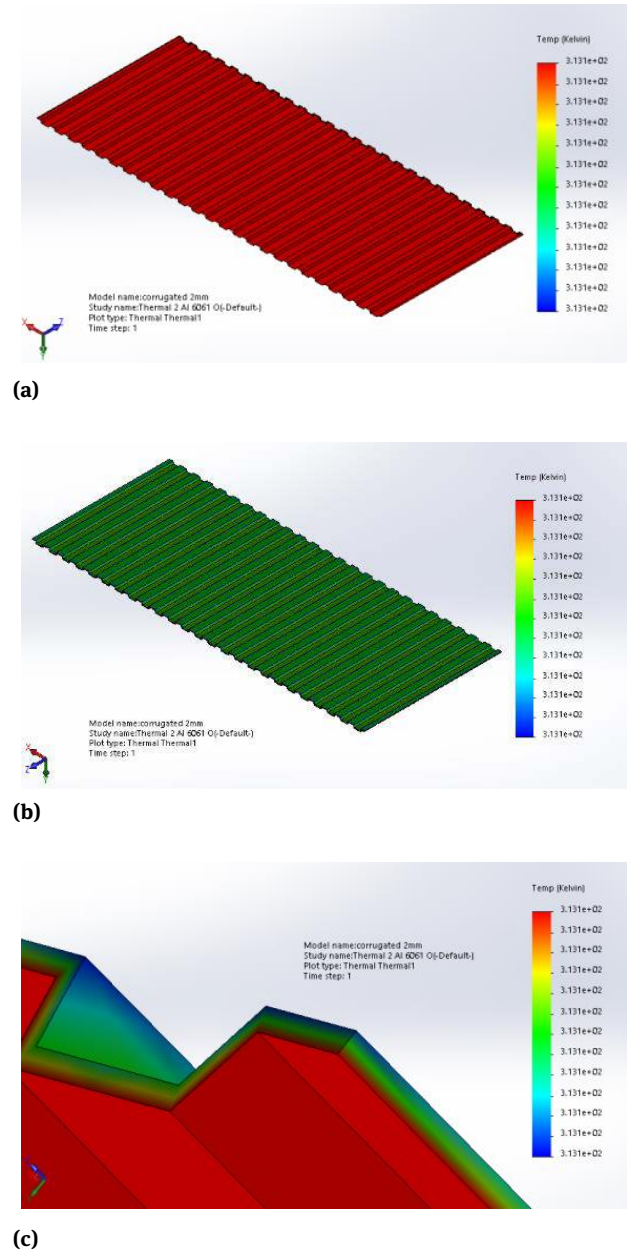
Figure 22: Result of the thermal simulation for the corrugated wall: (a) outer surface, (b) inner surface, and (c) edge

Figure 23: Result of the thermal simulation on the flat wall: (a) outer surface, (b) inner surface, (c) edge

3.2.6 Flat wall with a single stiffener

Figure 24 shows the thermal simulation results for the outer surface, inner surface, and edge of the panel, with aluminium 6061-O as the material. In the thermal simulation, the lowest value is 3.12E+05 Kelvin, and the highest value is 3.13E+05 Kelvin.
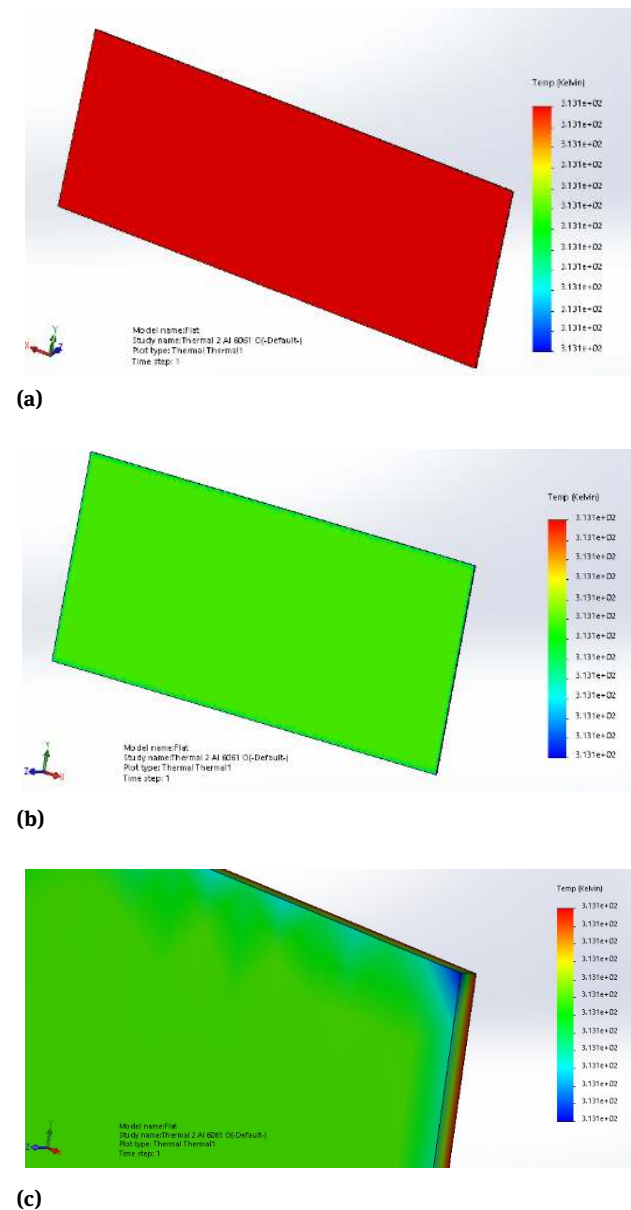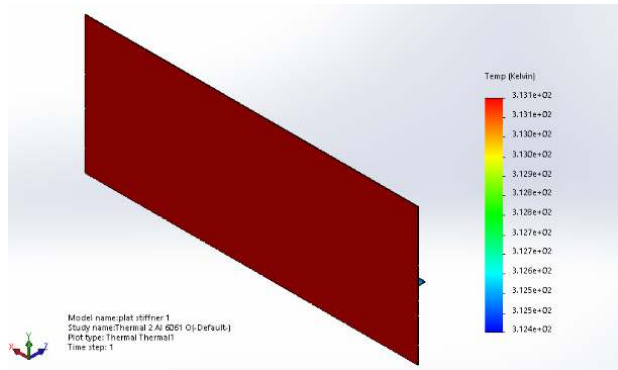
3.2.7 Flat wall with a cross stiffener

Figure 25 shows the thermal simulation results for the outer surface, inner surface, and edge of the panel, with aluminium 6061-O as the material. In the thermal simulation, the lowest value is 3.12E+05 Kelvin, and the highest value is 3.13E+05 Kelvin.
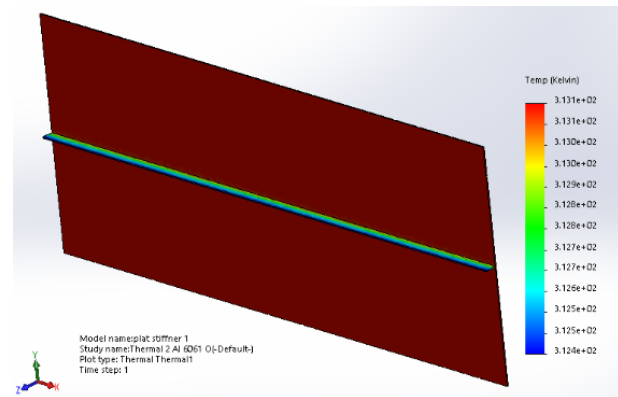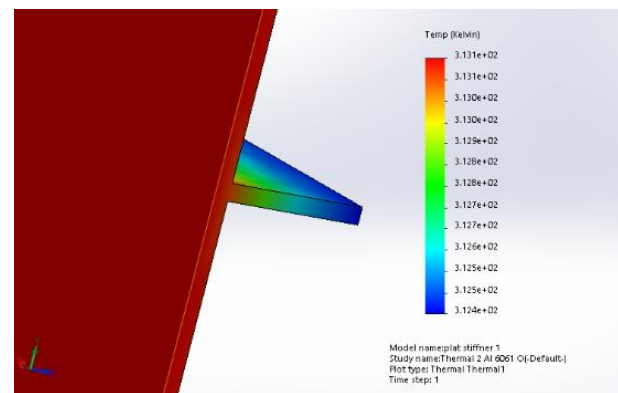

(a)

(b)

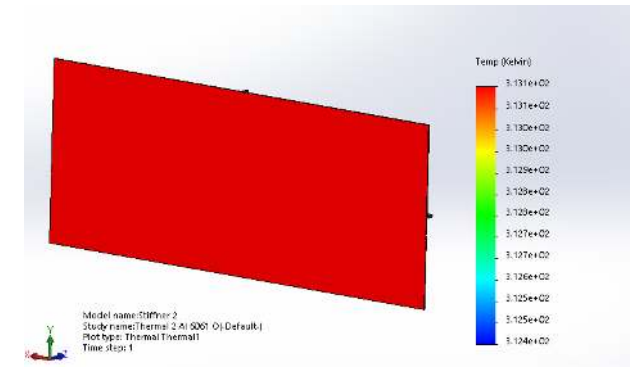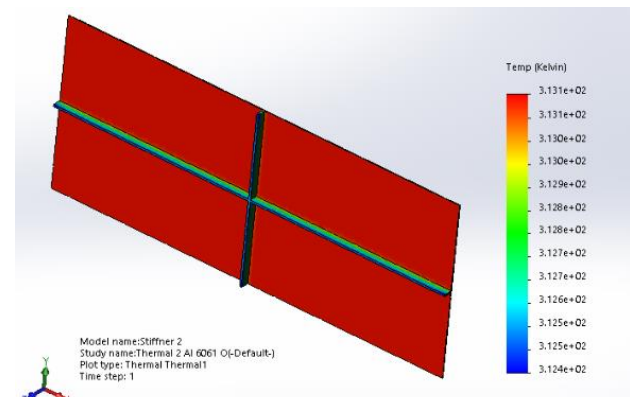

(c)

Figure 24: Result of the thermal simulation for the flat wall with a single stiffener: (a) outer surface, (b) inner surface, and (c) edge
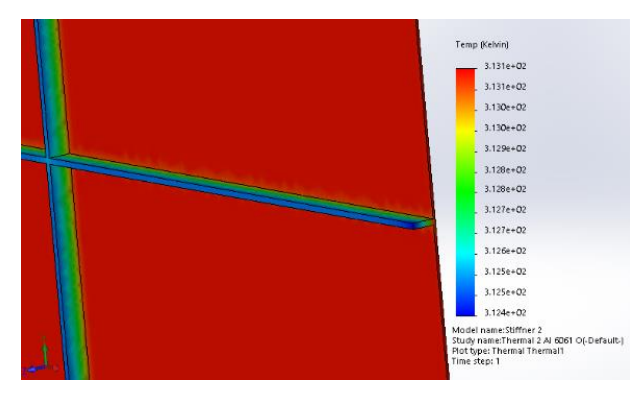

(a)

(b)

(c)

Figure 25: Result of the thermal simulation for the flat wall with a cross stiffener: (a) outer surface, (b) inner surface, (c) edge

3.3 Vibration analysis

3.3.1 General honeycomb

The simulation results in Figure 26 show the natural frequency values of the aluminium 6061-O honeycomb in mode shapes 1–5. Mode shapes 1–5 produce frequencies of 2.14E+01 Hz, 2.56E+01 Hz, 3.31E+01 Hz, 4.41E+01 Hz, and 5.72E+01 Hz, respectively.

3.3.2 Cross honeycomb

The simulation results in Figure 27 show the natural frequency of the cross honeycomb made of aluminium 6061-O in mode shapes 1–5. Mode shapes 1–5 produce frequency values of 4.34E+01 Hz, 5.23E+01 Hz, 6.92E+01 Hz, 9.45E+01 Hz, and 1.22E+02 Hz, respectively.

3.3.3 Square honeycomb

The simulation results in Figure 28 show the natural frequency of the square honeycomb made of aluminium 6061-O in mode shapes 1–5. Mode shapes 1–5 produce frequency values of 6.86E+01 Hz, 1.14E+02 Hz, 2.18E+02 Hz, 2.35E+02 Hz, and 2.40E+02 Hz, respectively.
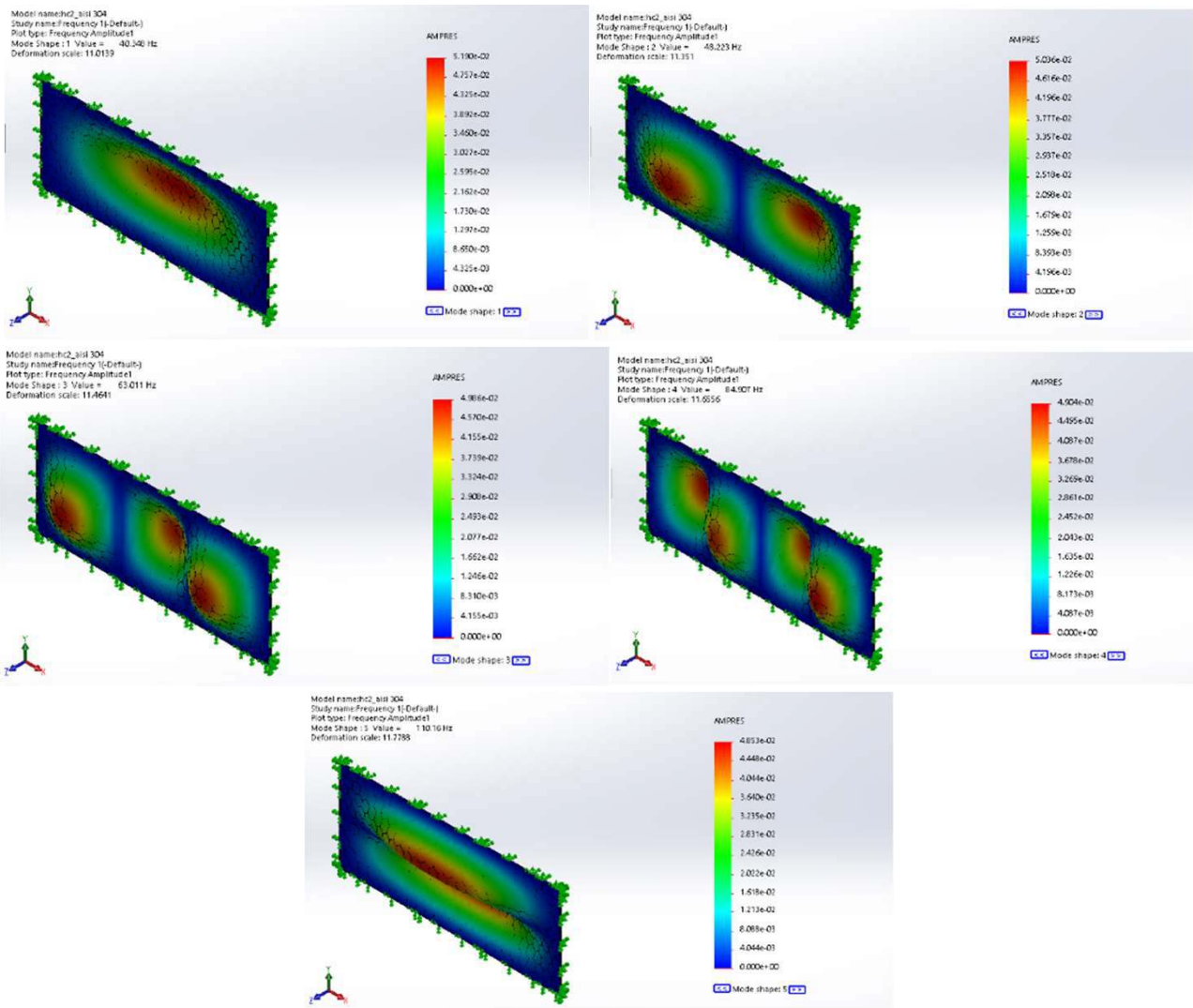
Figure 26: Mode shapes 1–5 of the general honeycomb
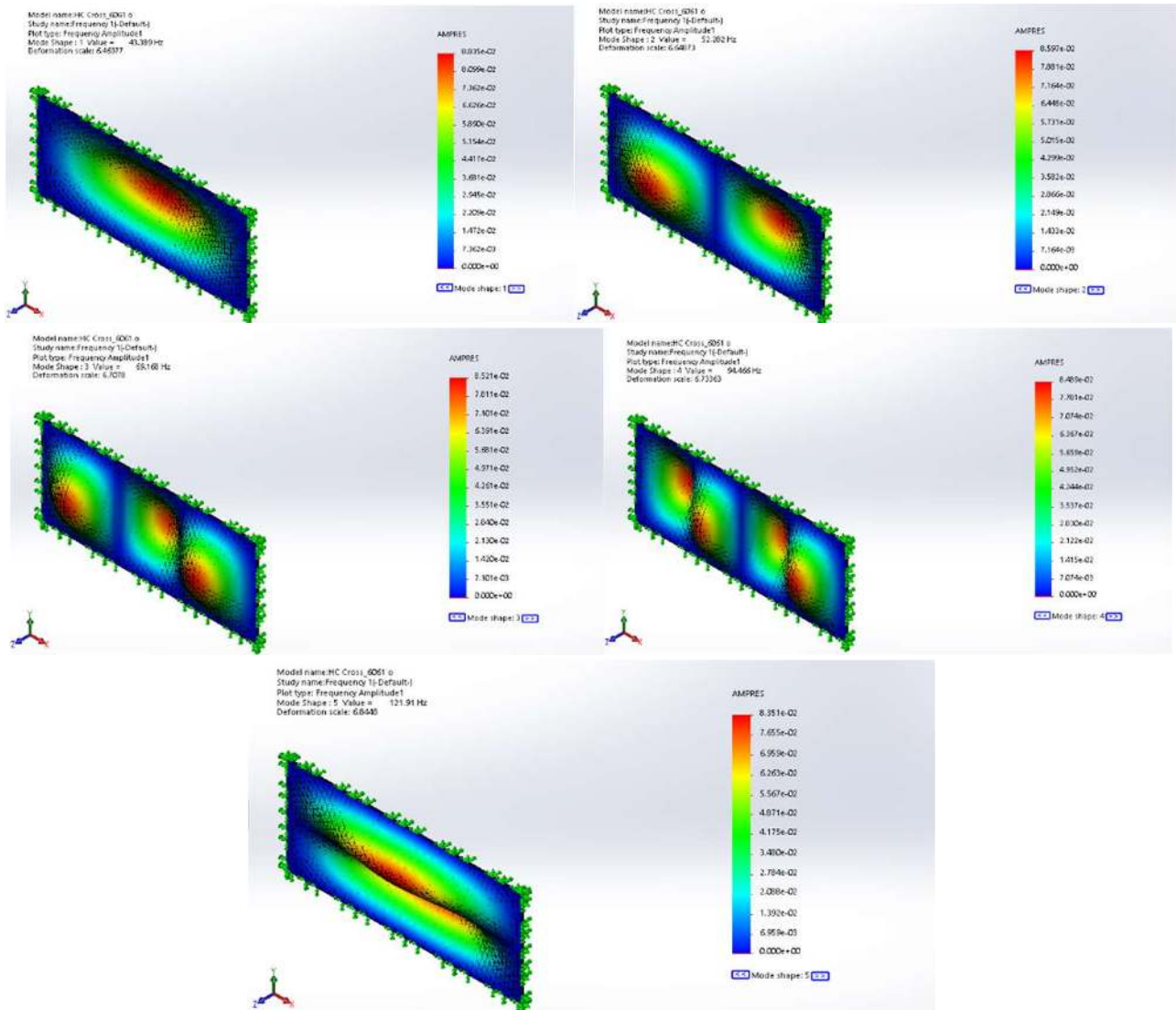
Figure 27: Mode shapes 1–5 of the cross honeycomb

3.3.4 Corrugated wall

The simulation results in Figure 29 show the natural frequency of the corrugated wall made of aluminium 6061-O in mode shapes 1–5. Mode shapes 1–5 produce frequency values of 6.15E+01 Hz, 5.42E+01 Hz, 5.56E+01 Hz, 5.80E+01 Hz, and 6.15E+01 Hz, respectively.

3.3.5 Flat wall

The simulation results in Figure 30 show the natural frequency of a flat wall made of aluminium 6061-O in mode shapes 1–5. Mode shapes 1–5 produce frequency values of 2.14E+01 Hz, 2.56E+01 Hz, 3.31E+01 Hz, 4.41E+01 Hz, and 5.72E+01 Hz, respectively.

3.3.6 Flat wall with a single stiffener

The simulation results in Figure 31 show the natural frequency of a flat wall with a stiffener made of aluminium 6061-O in mode shapes 1–5. Mode shapes 1–5 produce frequency values of 1.87E+01 Hz, 3.76E+01 Hz, 3.81E+01 Hz, 4.88E+01 Hz, and 6.05E+01 Hz, respectively.
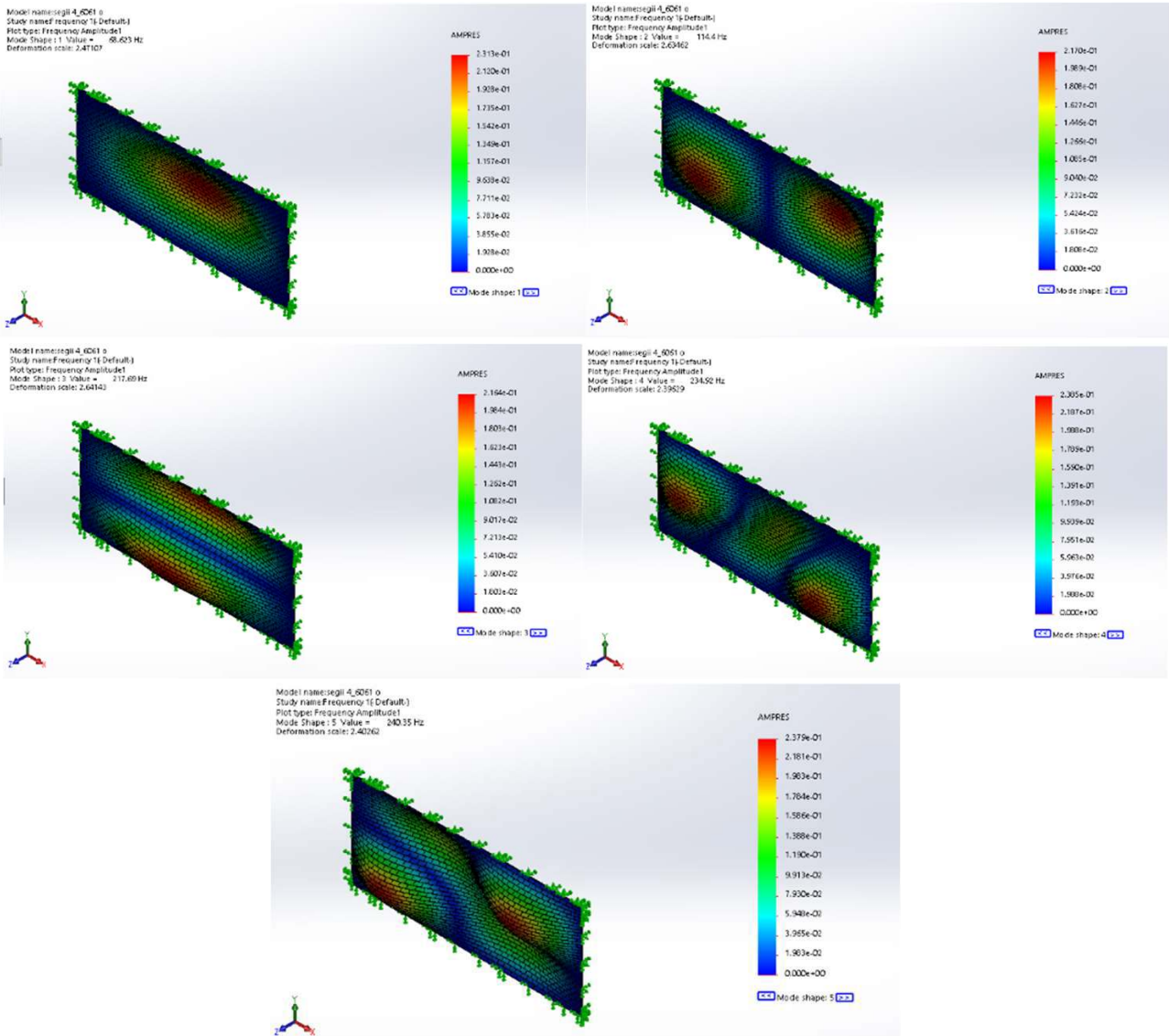
Figure 28: Mode shapes 1–5 of the square honeycomb
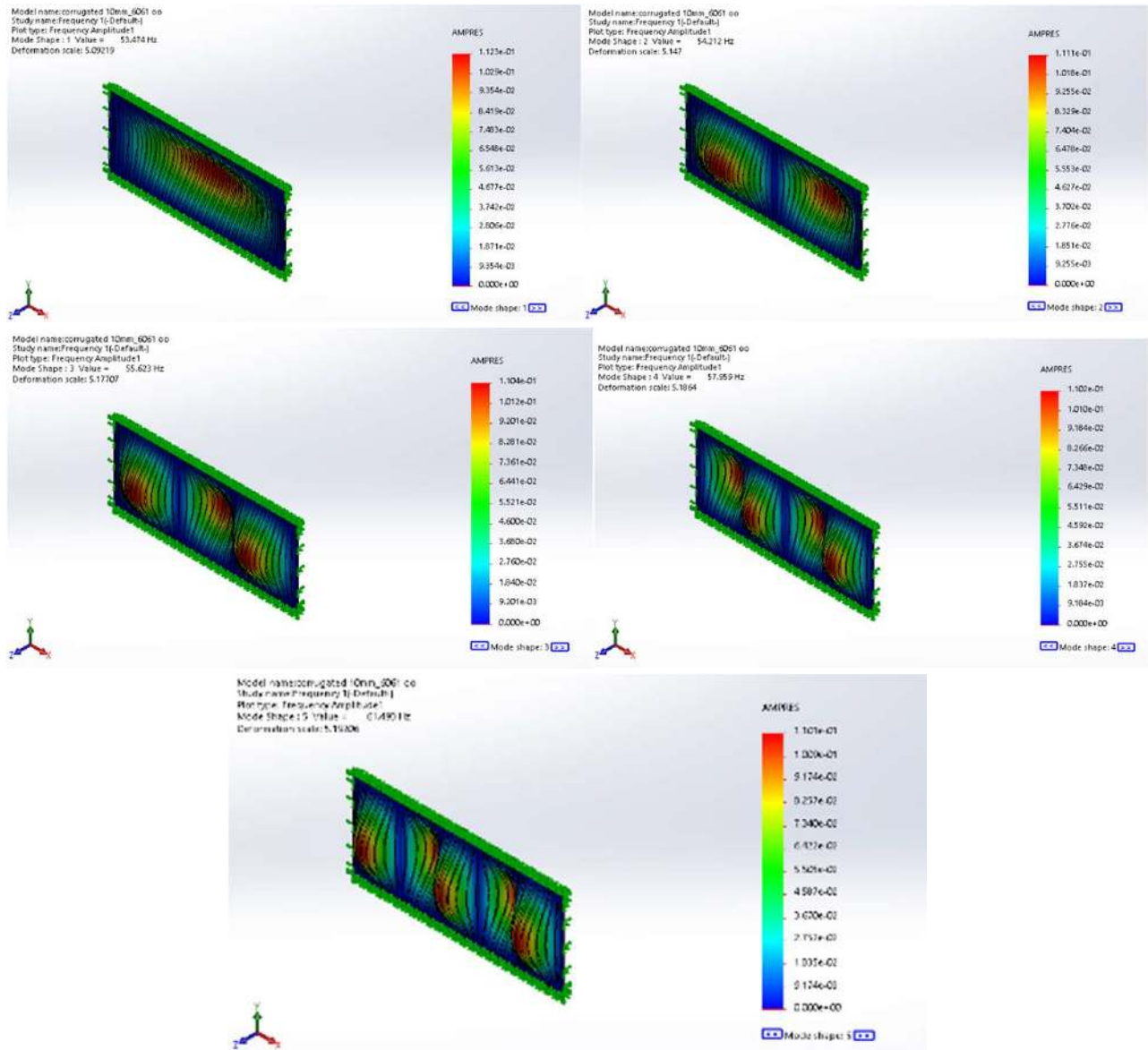
Figure 29: Mode shapes 1–5 of the corrugated wall
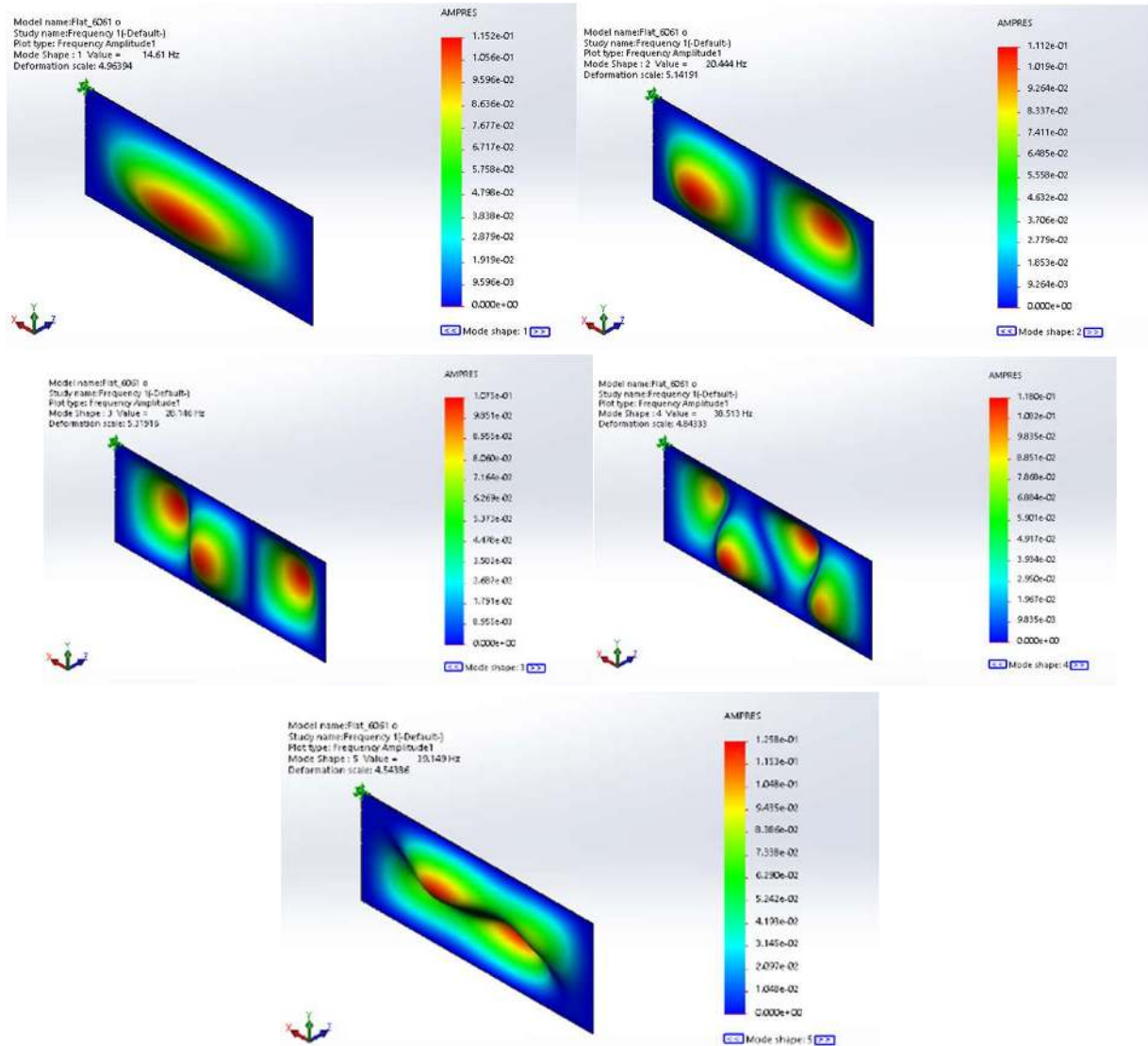
Figure 30: Mode shapes 1–5 of the flat wall

3.3.7 Flat wall with a cross stiffener

The simulation results in Figure 32 show the natural frequency of a flat wall with two stiffeners made of aluminium 6061-O in mode shapes 1–5. Mode shapes 1–5 produce frequency values of 4.32E+01 Hz, 4.43E+01 Hz, 4.76E+01 Hz, 4.91E+01 Hz, and 7.48E+01 Hz, respectively.

3.4 Buckling analysis

3.4.1 General honeycomb

Figure 33 shows the results of the buckling simulation for the general honeycomb made of aluminium 6061-O in mode shapes 1–4. For an applied load of 5.04E+05 N, the load factor values of the four modes are 1E+00, 1.94E+00, 5.68E+00, and 8.63E+00.

3.4.2 Cross honeycomb

The buckling simulation results for a cross honeycomb made of aluminum 6061-O in mode shapes 1–4 are shown in Figure 34. For an applied load of 5.11E+05 N, the load factor values of the four mode shapes are 1E+00, 1.93E+00, 5.60E+00, and 8.86E+00.
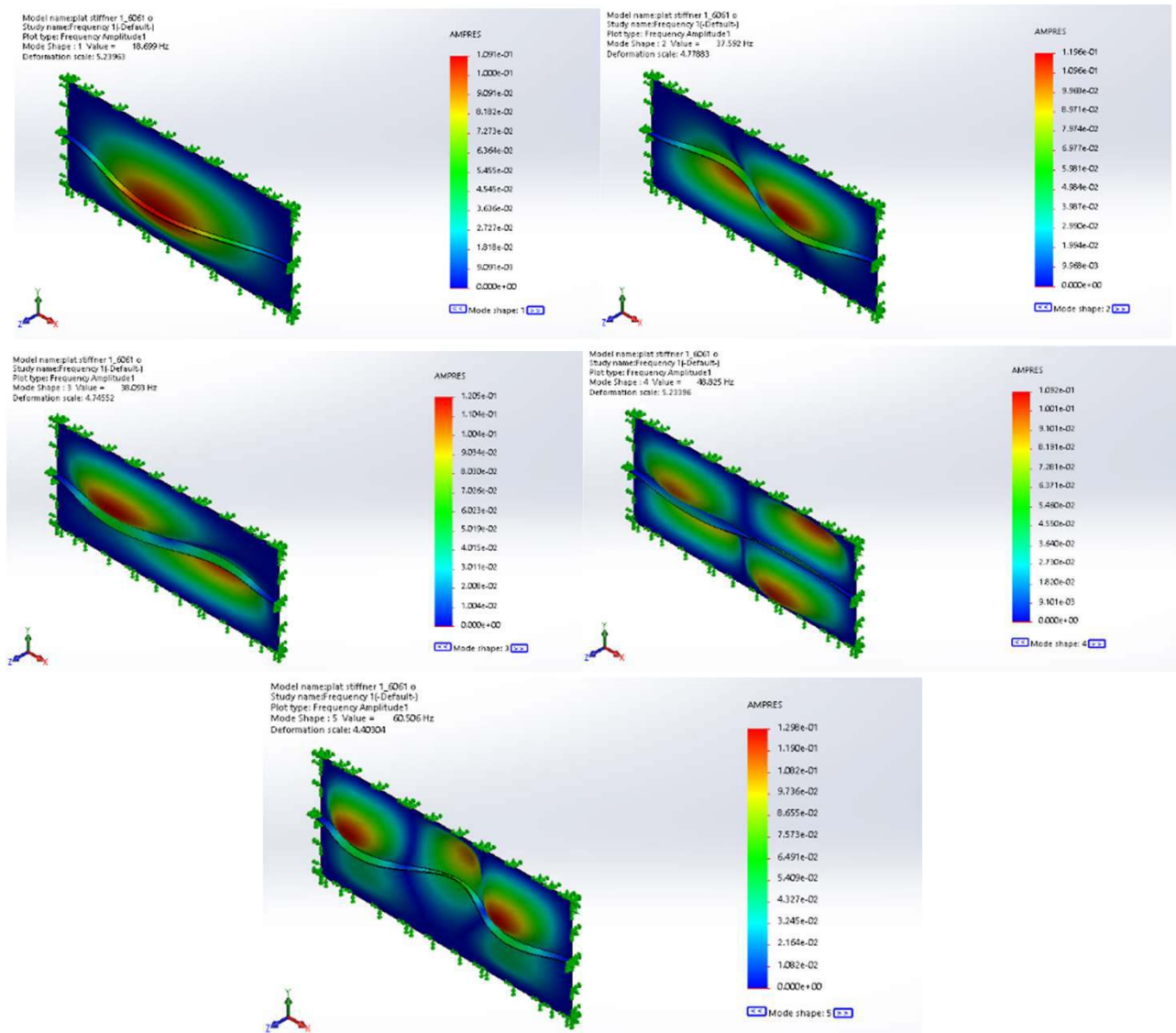
Figure 31: Mode shapes 1–5 of the flat wall a single stiffener
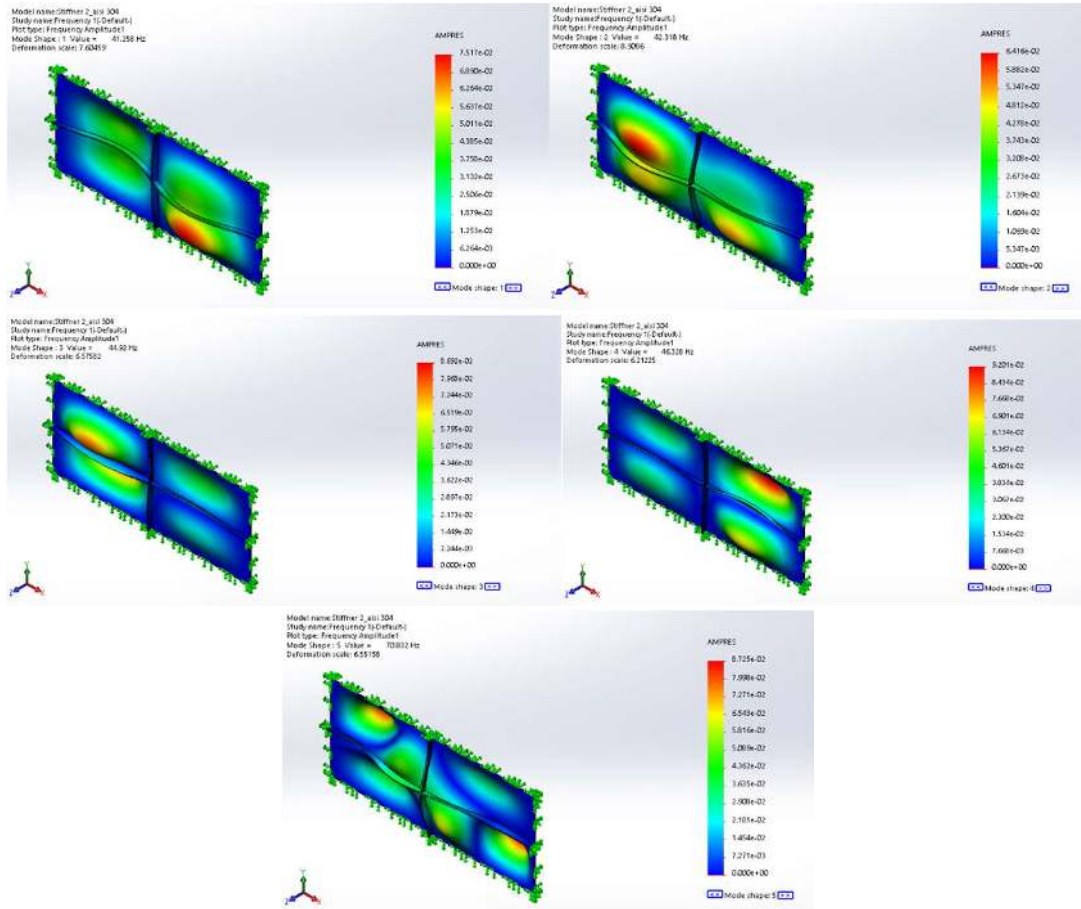
Figure 32: Mode shapes 1–5 of the flat wall with a cross stiffener
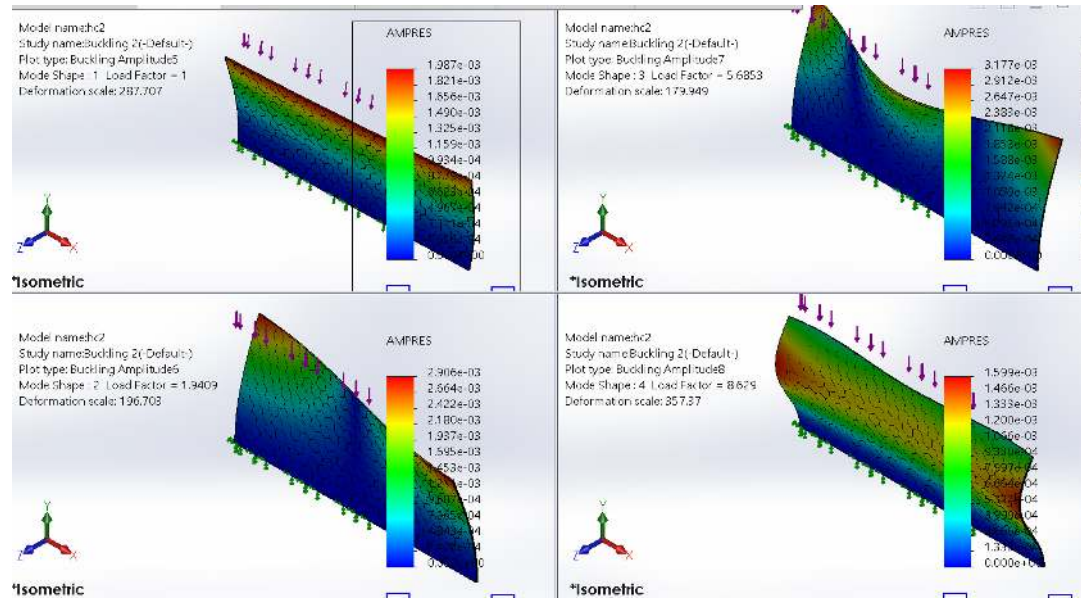
Figure 33: Buckling characteristics of the general honeycomb

3.4.3 Square honeycomb

Figure 35 shows the results of the buckling simulation for the square honeycomb made of aluminum 6061-O in mode shapes 1–4. For an applied load of 5.07E+05 N, the values of the load factor for the four modes are 1E+00, 1.93E+00, 5.64E+00, and 8.84E+00.

3.4.4 Corrugated wall

The results of the buckling simulation for the corrugated wall made of aluminium 6061-O in mode shapes 1–4 are shown in Figure 36. For an applied load of 5.90E+05 N, the load factor values of the four modes are 1E+00, 1.04E+00, 1.18E+00, and 1.55E+00.
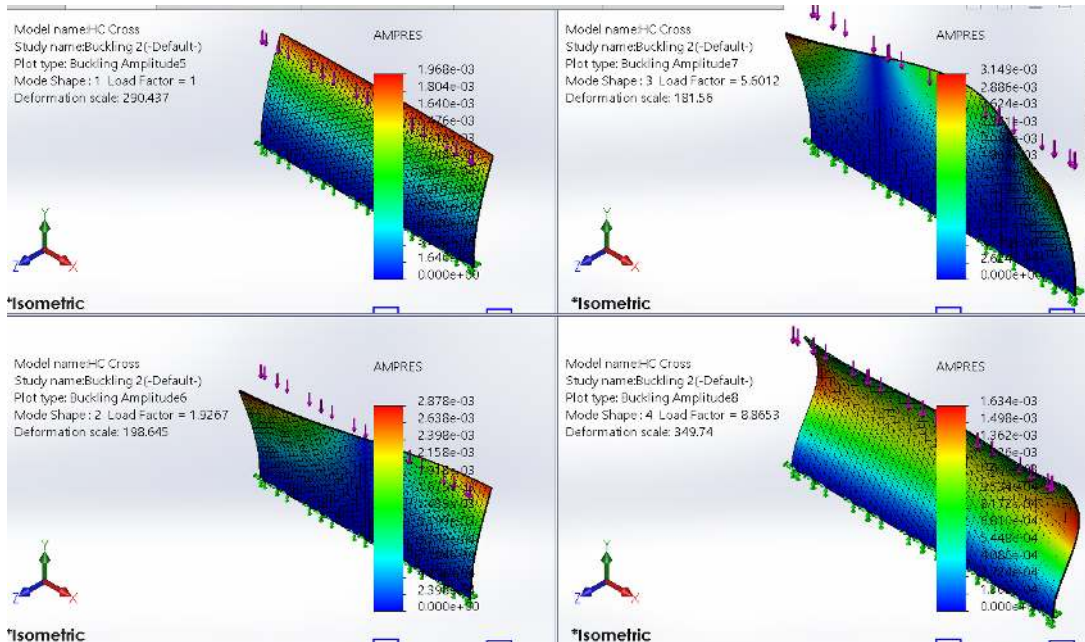
Figure 34: Buckling characteristics of the cross honeycomb
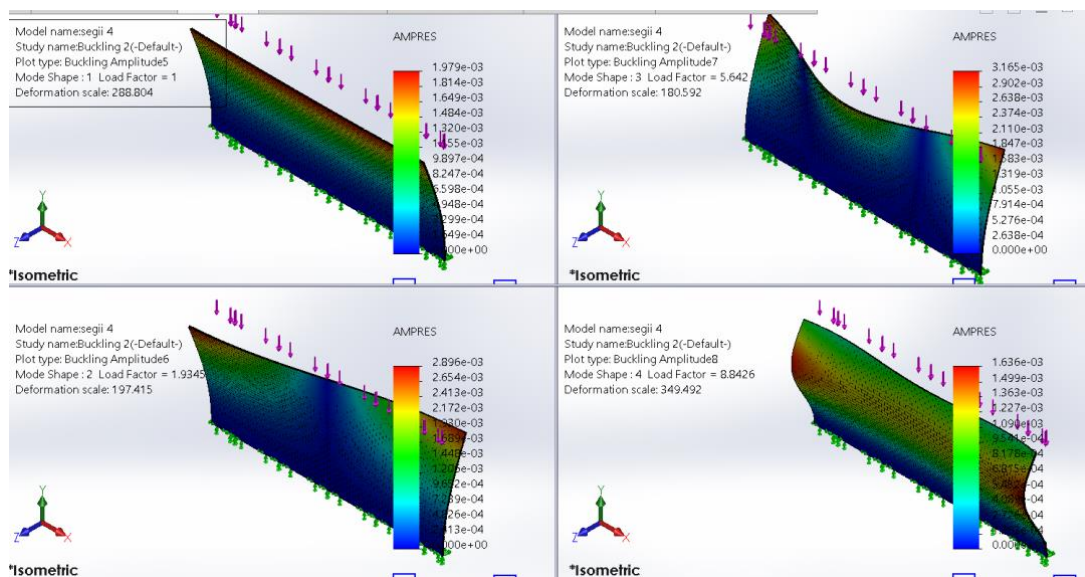
Figure 35: Buckling characteristics of the square honeycomb

3.4.5 Flat wall

The buckling simulation results for flat walls made of aluminum 6061-O in mode shapes 1–4 are shown in Figure 37. For an applied load of 2.79E+04 N, the load factor values of the four mode shapes are 1E+00, 1.93E+00, 5.65E+00, and 8.97E+00.

3.4.6 Flat wall with a single stiffener

Figure 38 shows the results of the buckling simulation for a flat wall with a single stiffener made of aluminium 6061-O in mode shapes 1–4. For an applied load of 2.84E+04 N, the factor values of the four mode shapes are 1E+00, 2.04E+00, 6.5E+00, and 9.03E+00.
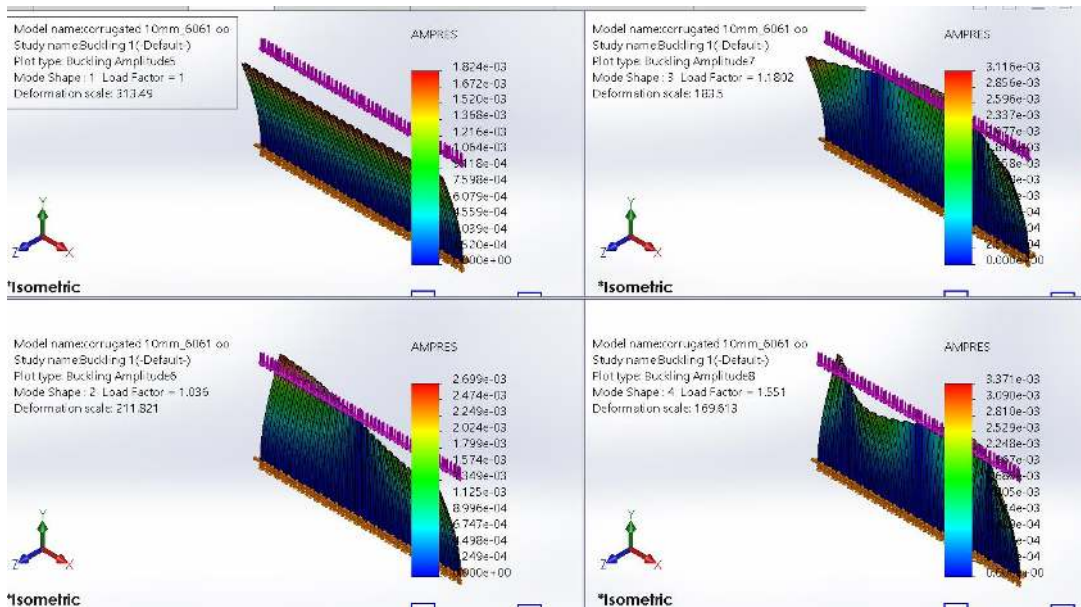
Figure 36: Buckling characteristics of the corrugated wall
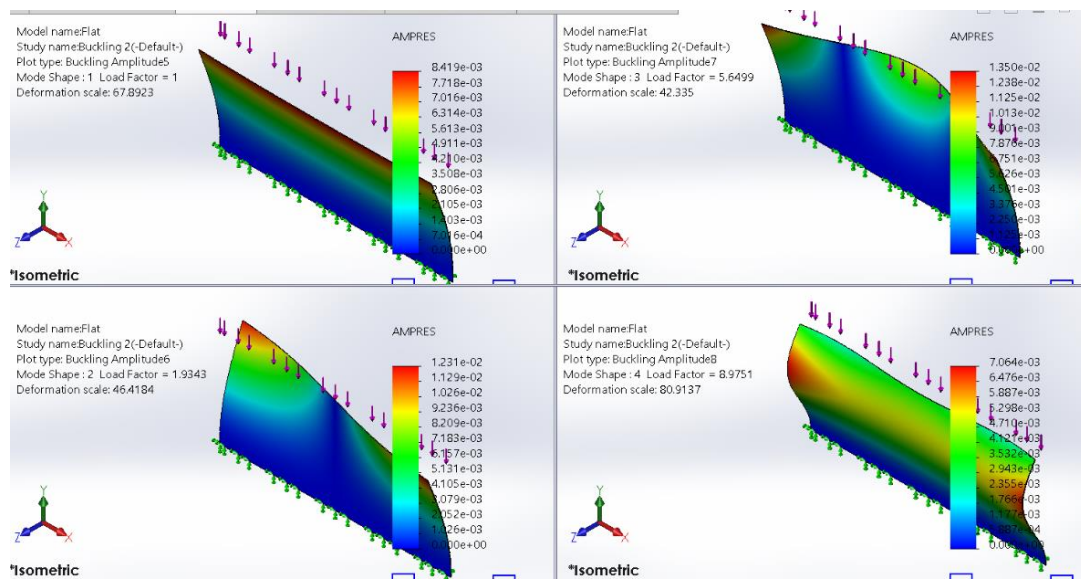
Figure 37: Buckling characteristics of the flat wall

3.4.7 Flat wall with a cross stiffener

Figure 39 shows the results of the buckling simulation for the flat wall with a cross stiffener made of aluminum 6061-O in mode shapes 1–4. For an applied load of 8.12E+04 N, the load factor values of the four mode shapes are 1E+00, 1.31E+00, 3.86E+00, and 5.56E+00.

4 Discussion

## 4.1 Static analysis

A static structural analysis was performed to evaluate the total deformation of the composite shell. Structural analyses are performed to examine stress, strain, and deformation in engineering structures that need to withstand mechanical and thermal loads. In this analysis, only mechanical loads were tested. Stress is related to the strength of the material of the body, and strain is a measure of the
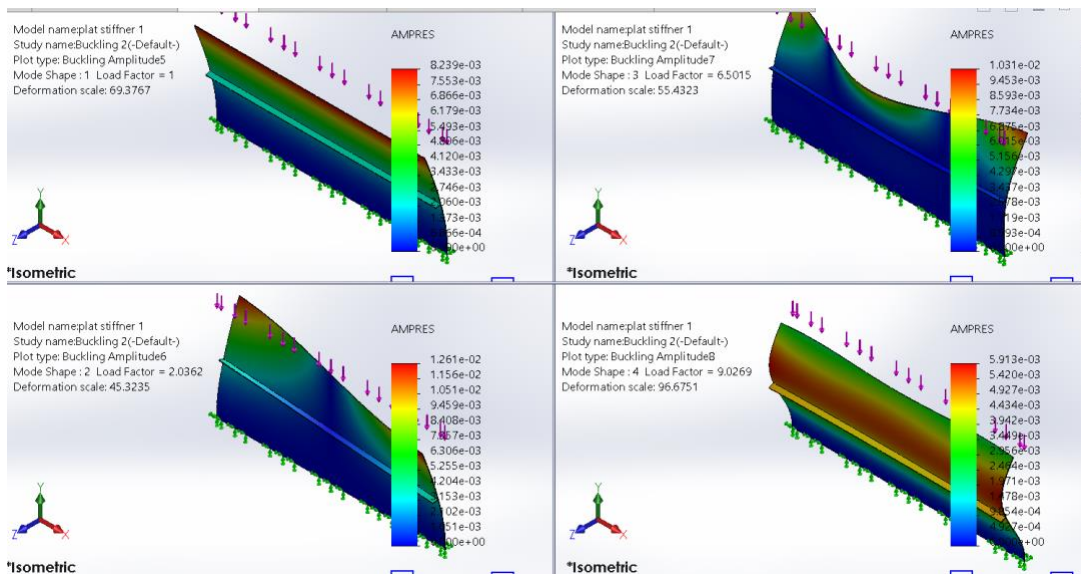
Figure 38: Buckling characteristics of the flat wall with a single stiffener
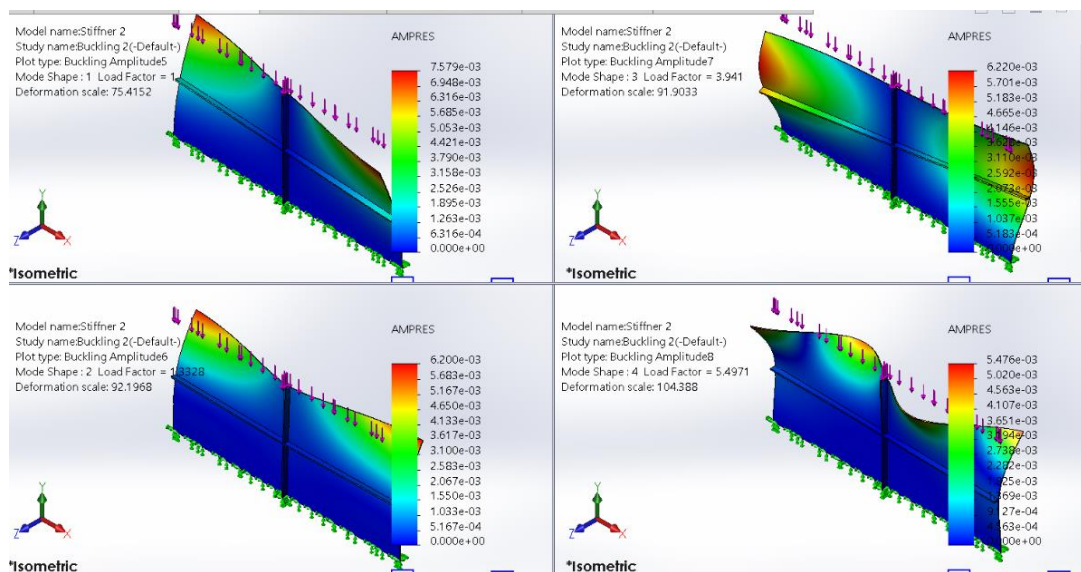
Figure 39: Buckling characteristics of the flat wall with a cross stiffener

deformation of the body. The application of force tends to change the shape and size of an object. This change is the deformation, which may be very obvious or barely noticeable. An increase in stress causes an increase in the strain ratio, a relationship known as Hooke's Law. The theory of small deflections is also used to investigate the behavior of linear elastic materials.

Displacement is the physical alteration that occurs in a material under a given loading stress. Displacement affects the safety and the life of the structure, where the more significant the stress, the greater the displacement, and the lower the safety level, and vice versa. In the static simulation, the more significant the thermal load, the greater the von Mises stress, strain, displacement, and safety factor.

Simulations were carried out using the SolidWorks application with the finite element method, and different materials were analyzed. The results of all static tests were obtained by carrying out simulations under a variety of considerations until the output values were stable. The temperature of the input thermal load was 308 Kelvin, which is based on the average between the container wall and ambient temperatures. Of the tested models, the corrugated core, which is made of aluminium 6061-O, produces the best results, as evidenced by a von Mises stress of 3.99E+04 N/mm^2, displacement of 1.39E+03 mm, strain of 3.75E−01, and safety factor of 1.55E+03. Conversely, the worst result is associated with the flat wall with a single stiffener, which has a von Mises stress of 2.23E+05 N/mm^2, displacement of 2.74E+04 mm, strain of 2.63E+00, and safety factor of 6.24E+04.

The static simulation was performed by adjusting the load until the critical load was obtained based on a buckling safety factor of 1. Among the tested models, the square honeycomb made of aluminum 6061-O produces the best results. This is evidenced by a critical load value of 3.40E+06 N. The worst result is obtained by the flat model, which has a critical load of 1.60E+06 N. The analyzed honeycomb structure is a sandwich panel, which has several advantages, including high strength and stiffness, good corrosion resistance, and relatively inexpensive production cost. As the main element and the content of the sandwich panel structure, the core plays a role in increasing the ability of the structure to absorb force, thereby increasing the strength of the material.

4.2 Thermal characteristics

The results of the thermal simulation for all models and variations are presented in Table 10, which reports the con-

vection heat transfer. The thermal simulation results (including thermal contours on previous sections) show that the best performance is obtained by container models with a honeycomb core (general, cross, or square) made of aluminium 6061-O, which has good convection heat transfer. This is evidenced by the maximum result obtained, which is 3.13E+05. The heat transfer takes place by convection. The results are influenced by the convection coefficient, which is calculated based on the thickness of each container model. Although the thermal simulation results are the same for the general honeycomb, cross honeycomb, and square honeycomb, it is necessary to consider the mass of each model, and the general honeycomb has the lowest mass. However, it can also be adjusted as needed for particular applications in the field.

For field applications that require slow heat transfer, a common practice is to store objects that are vulnerable to temperature changes in containers made of materials that can maintain their temperature stability. The production and maintenance costs of the container are important considerations, so aluminium 6061-O was chosen as the material in this study. Compared with low carbon steel A304 and aluminium 7075 T6, aluminium 6061-O is reasonably affordable, and the properties of the material are appropriate for the studied application.

The simulation output is the convection coefficient. The value of the convection coefficient was obtained on the basis of dry air properties, including thermal conductivity, the viscosity coefficient, the Prandtl number, and specific heat. These data were processed using formulas (6), (7), (8), and (9). In addition, the wall thickness affects the calculation. The wall thickness is directly proportional to the Reynolds and Nusselt numbers, whereas it is inversely proportional to the convection coefficient. Convection occurs when the Rayleigh number exceeds its critical value. The critical Rayleigh number can be estimated from the Nusselt number, which is one of the most critical parameters determined by natural convection heat transfer: a higher Nu number is obtained with an increase in load. Given a constant ambient temperature, an increase in load increases the temperature gradient of the container walls.

The properties of the material also affect the thermal simulation results. Thermal conductivity is a material property that indicates how quickly it conducts heat. An increase in the value of a fluid's thermal conductivity is due to the addition of particles that have a higher thermal conductivity than the fluid. The conductivity value represents the ease of thermal flow in a material and affects the temperature distribution throughout the material and the rate of heat transfer. The higher the conductivity, the lower the temperature for each point, but the more significant the

Table 10: Summary of the thermal simulation results based on the model variations

Model	Material	Min (Kelvin)	Max (Kelvin)
General honeycomb	A304	3.11E+05	3.13E+05
	6061-O	3.13E+05	3.13E+05
	7075 T6	3.13E+05	3.13E+05
Cross honeycomb	A304	3.12E+05	3.13E+05
	6061-O	3.13E+05	3.13E+05
	7075 T6	3.13E+05	3.13E+05
Square honeycomb	A304	3.12E+05	3.13E+05
	6061-O	3.13E+05	3.13E+05
	7075 T6	3.13E+05	3.13E+05
Corrugated	A304	3.13E+05	3.13E+05
	6061-O	3.13E+05	3.13E+05
	7075 T6	3.13E+05	3.13E+05
Flat	A304	3.13E+05	3.13E+05
	6061-O	3.13E+05	3.13E+05
	7075 T6	3.13E+05	3.13E+05
Flat with single stiffener	A304	3.10E+05	3.13E+05
	6061-O	3.12E+05	3.13E+05
	7075 T6	3.12E+05	3.13E+05
Flat with cross stiffener	A304	3.08E+05	3.13E+05
	6061-O	3.12E+05	3.13E+05
	7075 T6	3.12E+05	3.13E+05
Mean		3.12E+05	3.13E+05
Median		3.13E+05	3.13E+05
Sample variance		1.10E+06	2.45E+03
Standard deviation		1.37E+03	4.95E+01
Variance coeff. (%)		4.38.E−03	1.58E−04
Standard error		2.98E+02	1.08E+01

transfer rate. The incoming air velocity also affects the temperature distribution throughout the material and the rate of heat transfer. The higher the air velocity, the greater the temperature and heat transfer rate, and the greater the effect of air on the Reynolds number. The simulation results show that, if the air velocity is assumed to be 0.3 m/s, then the value obtained is not very significant.

4.3 Vibration behavior

The vibration simulation results are shown in Table 11, which contains the entire simulation dataset. The results of the vibration simulation carried out on structures made of aluminum 6061-O show that, of the four mode shapes, the four-sided model obtains the highest average frequency, which is 3.51E+02 Hz, and the flat model has the lowest value, which is 7.14E+01 Hz. The reason for this is

that the square honeycomb has many gaps in the core and sandwich-shaped plate that effectively absorb vibrations.

The results of the vibration simulation are reported for five mode shapes with different natural frequency values. Each mode shape has a different form of vibration because the external force is distributed differently in the material, which affects its ability to absorb these forces. The frequency also tends to vary between mode shapes because the boundary conditions are different, which affects the natural frequency value. The frequency tends to increase from mode shape 1 to mode shape 5 due to the increasing length of vibrational waves. The greater the frequency, the greater the amplitude. Of the five models, the four-sided model is best at absorbing these forces because the direction of the force resulting from external vibrations can be evenly distributed throughout the structure. This even distribution occurs because the quadrilateral shape has a cavity in the core so it can effectively absorb vibrations. However, in models other than the honeycomb that do not have

Table 11: Summary of the vibration analysis

Model	Material	Mode Shape 1 Frequency (Hertz)	Model	Material	Mode Shape 2 Frequency (Hertz)
General honeycomb	A304	4.03E+01	General honeycomb	A304	4.82E+01
	6061-O	4.26E+01		6061-O	5.09E+01
	7075 T6	4.26E+01		7075 T6	5.09E+01
Cross honeycomb	A304	4.11E+01	Cross honeycomb	A304	4.95E+01
	6061-O	4.34E+01		6061-O	5.23E+01
	7075 T6	4.34E+01		7075 T6	5.24E+01
Square honeycomb	A304	6.36E+01	Square honeycomb	A304	1.07E+02
	6061-O	6.86E+01		6061-O	1.14E+02
	7075 T6	6.87E+01		7075 T6	1.15E+02
Corrugated	A304	5.14E+01	Corrugated	A304	5.21E+01
	6061-O	5.35E+01		6061-O	5.42E+01
	7075 T6	5.35E+01		7075 T6	5.43E+01
Flat	A304	2.03E+01	Flat	A304	2.42E+01
	6061-O	2.14E+01		6061-O	2.56E+01
	7075 T6	2.14E+01		7075 T6	2.56E+01
Flat with single stiffener	A304	1.78E+01	Flat with single stiffener	A304	3.57E+01
	6061-O	1.87E+01		6061-O	3.76E+01
	7075 T6	1.83E+01		7075 T6	3.76E+01
Flat with cross stiffener	A304	4.13E+01	Flat with cross stiffener	A304	4.23E+01
	6061-O	4.32E+01		6061-O	4.43E+01
	7075 T6	4.33E+01		7075 T6	4.43E+01

Model	Material	Mode Shape 3 Frequency (Hertz)	Model	Material	Mode Shape 4 Frequency (Hertz)
General honeycomb	A 304	6.30E+01	General honeycomb	A304	8.49E+01
	6061-O	6.65E+01		6061-O	8.97E+01
	7075 T6	6.66E+01		7075 T6	8.98E+01
Cross honeycomb	A 304	6.54E+01	Cross honeycomb	A304	8.92E+01
	6061-O	6.92E+01		6061-O	9.45E+01
	7075 T6	6.93E+01		7075 T6	9.46E+01
Square honeycomb	A 304	2.03E+02	Square honeycomb	A304	2.18E+02
	6061-O	2.18E+02		6061-O	2.35E+02
	7075 T6	2.18E+02		7075 T6	2.35E+02
Corrugated	A 304	5.35E+01	Corrugated	A304	5.57E+01
	6061-O	5.56E+01		6061-O	5.80E+01
	7075 T6	5.57E+01		7075 T6	5.80E+01
Flat	A 304	3.14E+01	Flat	A304	4.19E+01
	6061-O	3.31E+01		6061-O	4.41E+01
	7075 T6	3.31E+01		7075 T6	4.42E+01
Flat with single stiffener	A 304	3.62E+01	Flat with single stiffener	A304	4.58E+01
	6061-O	3.81E+01		6061-O	4.88E+01
	7075 T6	3.81E+01		7075 T6	4.89E+01
Flat with cross stiffener	A 304	4.49E+01	Flat with cross stiffener	A304	4.63E+01
	6061-O	4.76E+01		6061-O	4.91E+01
	7075 T6	4.77E+01		7075 T6	4.92E+01

Table 11: ... continued

Model	Material	Mode Shape 5 Frequency (Hertz)
General honeycomb	A 304	1.10E+02
	6061-O	1.16E+02
	7075 T6	1.17E+02
Cross honeycomb	A 304	1.15E+02
	6061-O	1.22E+02
	7075 T6	1.22E+02
Square honeycomb	A 304	2.24E+02
	6061-O	2.40E+02
	7075 T6	2.41E+02
Corrugated	A 304	5.90E+01
	6061-O	6.15E+01
	7075 T6	6.16E+01
Flat	A 304	5.42E+01
	6061-O	5.72E+01
	7075 T6	5.73E+01
Flat with single stiffener	A 304	5.73E+01
	6061-O	6.05E+01
	7075 T6	6.06E+01
Flat with cross stiffener	A 304	7.08E+01
	6061-O	7.48E+01
	7075 T6	7.49E+01

a cavity in the core, the maximum frequency tends to be low because the vibrations are not evenly distributed, so the stress is concentrated at a few points, which can reduce the performance of the material.

The different simulation results based on mode shape show the possible scenarios that may occur in reality when the container is loaded onto a ship; of course, the container will experience varying vibrations from different sources. An important objective of simulating the mode shape is to determine the maximum frequency that can be absorbed by the structure. Once the maximum value is known, further optimization can be carried out, or new models can be constructed with better vibration absorption. The maximum frequency obtained for each mode shape shows the ability to absorb vibration and resist deformation. The frequency can be reduced by the addition of rubber material because it can absorb vibrations very effectively, so it can be used in the outer layer of containers that come into contact with other containers. In addition to its ability to absorb vibration, rubber is also widely used because it is light.

The static simulation was performed by adjusting the load until the critical load was obtained based on a buckling safety factor of 1. The results show that the square honeycomb made of aluminium material 6061-O has the best results, as evidenced by its critical load of 3.40E+06 N. Conversely, the worst result is obtained by the flat model, which has a critical load of 1.60E+06 N. This result is explained by the many gaps in the core and plate in the sandwich construction of the square honeycomb, which can effectively dampen vibrations.

4.4 Buckling pattern

Core plates under compression and/or shear loading are sensitive to buckling failures. When the load reaches a critical value, the member no longer remains straight but deflects sideways at a more or less constant value of the load. Analysis of the idealized behavior sheds light on the real structural problem of buckling columns. Buckling describes the process of switching from the straight, stiff configuration to a bent one that has very low stiffness. The load at which this transformation takes place is the critical buckling load.

The critical buckling load can be predicted by calculating the eigenvalues of the structure based on the specified properties. In this study, finite element analysis was performed to obtain linear buckling results. The results of the linear-buckling or eigenvalue buckling analysis on a single column only rest on the bottom. The critical load can also be calculated based on Euler's formula in Equation (13). The column data in Table 12 reveal that the buckling simulation results are different among the models. The corrugated model made of aluminum 6061-O has the highest critical load of 5.90E+05 N, while the flat model has the lowest critical load of 2.79E+04 N for mode shape 1. The critical loads are greater for mode shapes 2, 3, and 4, which determines mode shape 1. This shows that the critical load of the container wall is affected not only by the thickness of the wall but also by its structural shape. These results were also obtained by adjusting the load until the critical load was obtained based on a buckling factor of safety of 1, which is an indicator of the safety against buckling or the ratio of the buckling load to the applied load.

Modes 1 and 2 are identical and represent a repeated mode: any arbitrary axial orientation of the fundamental shape is possible. Modes 3 and 4 are also repeated roots. The implication is that any small variation in boundary conditions, component details, or load eccentricity can cause any of the modes to occur. The modes are completely independent in the linear analysis; thus, mode 1 or 2 or 3,

Table 12: Summary of the results for the buckling factor of safety

Model	Material	Mode shape	Force (N)	Buckling factor of safety
General honeycomb	A304	1	1.36E+06	1.00E+00
		2		2.00E+00
		3		5.95E+00
		4		8.65E+00
	6061-O	1	5.04E+05	1.00E+00
		2		1.94E+00
		3		5.69E+00
		4		8.63E+00
	7075 T6	1	5.25E+05	1.00E+00
		2		1.94E+00
		3		5.69E+00
		4		8.63E+00
Cross honeycomb	A304	1	1.37E+06	1.00E+00
		2		1.99E+00
		3		5.87E+00
		4		8.89E+00
	6061-O	1	5.11E+05	1.00E+00
		2		1.93E+00
		3		5.60E+00
		4		8.87E+00
	7075 T6	1	5.33E+05	1.00E+00
		2		1.93E+00
		3		5.60E+00
		4		8.87E+00
Square honeycomb	A304	1	1.36E+06	1.00E+00
		2		2.00E+00
		3		5.91E+00
		4		8.86E+00
	6061-O	1	5.07E+05	1.00E+00
		2		2.09E+00
		3		7.28E+00
		4		1.04E+01
	7075 T6	1	5.29E+05	1.00E+00
		2		2.09E+00
		3		7.28E+00
		4		1.04E+01
Corrugated	A304	1	1.62E+06	1.00E+00
		2		1.04E+00
		3		1.18E+00
		4		1.56E+00
	6061-O	1	5.90E+05	1.00E+00
		2		1.04E+00
		3		1.18E+00
		4		1.55E+00
	7075 T6	1	6.16E+05	1.00E+00
		2		1.03E+00
		3		1.18E+00
		4		1.55E+00

Table 12: ... continued

Model	Material	Mode shape	Force (N)	Buckling factor of safety
Flat	A304	1	7.50E+04	1.00E+00
		2		2.00E+00
		3		5.92E+00
		4		9.00E+00
	6061-O	1	2.79E+04	1.00E+00
		2		1.93E+00
		3		5.65E+00
		4		8.98E+00
	7075 T6	1	2.91E+04	1.00E+00
		2		1.93E+00
		3		5.65E+00
		4		8.97E+00
Flat with single stiffener	A304	1	7.61E+04	1.00E+00
		2		2.10E+00
		3		6.78E+00
		4		9.03E+00
	6061-O	1	2.84E+04	1.00E+00
		2		2.04E+00
		3		6.50E+00
		4		9.03E+00
	7075 T6	1	2.96E+04	1.00E+00
		2		2.04E+00
		3		6.50E+00
		4		9.03E+00
Flat with cross stiffener	A304	1	2.26E+05	1.00E+00
		2		1.31E+00
		3		3.86E+00
		4		5.56E+00
	6061-O	1	8.12E+04	1.00E+00
		2		1.33E+00
		3		3.94E+00
		4		5.50E+00
	7075 T6	1	8.47E+04	1.00E+00
		2		1.33E+00
		3		3.94E+00
		4		5.50E+00

etc., can occur. One of the practical implications is that if mode pair 1 and 2 were not possible due to snubbing against adjacent components, for example, then mode pair 3 and 4 could occur. It is important to assess the classifications of higher mode shapes and eigenvalues to identify any practical implications for the response. However, there may be only one dominant first mode, with the next set of modes completely infeasible and having very high critical loads. These can be ignored. These results demonstrate that applying the corrugated wall model to a shipping container in practical situations can improve its ability to withstand buckling when stacked because its critical load is increased.

5 Conclusions

This work was conducted to analyze several proposed panel geometries of a shipping container for potential new designs. A number of physical loadings were applied to

panels, *i.e.*, static, vibration, buckling, and thermal. Based on the analyses, the findings are summarized as follows:

– The static simulation shows that the corrugated design has the best performance compared with other models. Corrugated walls are generally used for containers for this reason. However, in the simulation, the square honeycomb model has the best vibration characteristics, with an average frequency of 3.51E+02 Hz. The static strength of the square honeycomb is not much different from that of the corrugated design, but its ability to absorb vibrations is the best among the analyzed models. This could form the basis for further research on containers with square honeycomb walls.

– The square honeycomb also outperforms the other models when it is assessed in terms of the factor of safety. However, in the buckling simulation, the best critical load strength is obtained by the corrugated model, with a value of 5.90E+05 N.

– Based on the thermal analysis, the recommended model is the square honeycomb. From the evaluation, the von Mises stress is 8.34E+04 N/mm^2, the displacement is 1.39E+03 mm, and the safety factor is 4.76E+05. Furthermore, in the thermal simulation, the results for the honeycomb core are better than those of the other core models. The maximum convection heat transfer is 3.13E+05.

– The static strength of the square honeycomb is not much different from that of the corrugated design, but the former has the best critical load. This could form the basis for further research on containers with square honeycomb walls.

– The findings of this research can be used as a reference for future design considerations in the manufacturing of shipping containers. These results demonstrate that the container performance and characteristics can be adjusted according to the needs of the market and operational demands.

Author contributions: All authors have accepted responsibility for the entire content of this manuscript and approved its submission.

Conflict of interest: The authors state no conflict of interest.

References

[1] Prabowo AR, Laksono FB, Sohn JM. Investigation of structural performance subjected to impact loading using finite element approach: case of ship-container collision. Curved Layered Struct. 2020; 7: 17-28.

[2] Rozylo P. Failure analysis of thin-walled composite structures using independent advanced damage models. Composite. Struct. 2021; 113598.

[3] Prabowo AR, Do QT, Cao B, Bae DM. Land and marine-based structures subjected to explosion loading: a review on critical transportation and infrastructure. Proc. Struct. Int. 2020; 27: 77-84.

[4] Shariati M, Farzi G, Dadrasi A. Mechanical properties and energy absorption capability of thin-walled square columns of silica/epoxy nanocomposite. Const. Build. Mat. 2015; 78: 362-368.

[5] Prabowo AR, Bae DM. Environmental risk of maritime territory subjected to accidental phenomena: Correlation of oil spill and ship grounding in the Exxon Valdez's case. Res. Eng. 2019; 100035.

[6] Gagnon RE, Wang J. Numerical simulations of a tanker collision with a bergy bit incorporating hydrodynamics, a validated ice model and damage to the vessel. Cold Reg. Sci. Tech. 2012; 81: 26-35.

[7] Prabowo AR, Cao B, Sohn JM, Bae DM. Crashworthiness assessment of thin-walled double bottom tanker: Influences of seabed to structural damage and damage-energy formulae for grounding damage calculations. J. Ocean Eng. Sci. 2020; 5: 387-400

[8] Ross CTF, Köster P, Little APF. Tewkesbury, G. Vibration of a thin-walled prolate dome under external water pressure. Ocean Eng. 2007; 3-4: 560-575.

[9] Kitarovic S, Zanic V. Approximate approach to progressive collapse analysis of the monotonous thin-walled structures in vertical bending. Mar. Struct. 2014; 39: 255-286.

[10] Smaradhana DF, Prabowo AR, Ganda ANF. Exploring the potential of graphene materials in marine and shipping industries – A technical review for prospective application on ship operation and material-structure aspects. J. Ocean Eng. Sci. 2021; in press [https://doi.org/10.1016/j.joes.2021.02.004]

[11] Marine Department H. Ranking of Container Ports of the World. 2007; 743. http://www.mardep.gov.hk/en/publication/pdf/portstat_2_y_b5.pdf

[12] UNCTAD. Reveiw of Maritime Transport. In United Nations Conference on Trade and Development. 2018. https://unctad.org/en/PublicationsLibrary/rmt2018_en.pdf

[13] Patel H, Panchal KC, Jadav CS. Structural analysis of truck chassis frame and design optimization for weight reduction. Int. J. Eng. Adv. Technol. 2013; 2: 665-668.

[14] Merneedi A, RaoNalluri, M, Rao VS. Free vibration analysis of a thin rectangular plate with multiple circular and rectangular cut-outs. Int. J. Eng. Adv. Technol. 2017; 31: 5085-5202.

[15] Vogel D, Wehmeyer M, Kebbach M, Heyer H, Bader R. Stress and strain distribution in femoral heads for hip resurfacing arthroplasty with different materials: a finite element analysis. J. Mech. Behav. Biomed. Mater. 2021; 113: 104-115.

[16] Goodnow F, Zaluzec M. 2005 Ford GT - melding the past and the future. SAE Tech. Pap. 2004; 724.

[17] Pan J, Fang H, Xu MC, Wu YF. Study on the performance of energy absorption structure of bridge piers against vehicle collision.

Thin-Walled Struct. 2018; 130: 85-100.

[18] Segalman DJ, Fulcher CW, Reese GM, Field Jr RV. An efficient method for calculating rms Von-Mises stress in a random vibration environment. J. Sound Vib.2000; 2: 393-410.

[19] Røsdal A. Analysis and optimization of sandwich panels. Master's thesis, UiT Norges arktiske universitet, 2017.

[20] DIABgroup. Guide to Core and Sandwich, 1st ed.; DIABgroup: Laholm, Sweden.2012; pp.1-48.

[21] Ramnath BV, Alagarraja K, Elanchezhian C. Review on sandwich composite and their applications. Mater. Today Proc. 2019; 16: 859-864.

[22] Chawa PK, Mukkamala SK. Design and analysis of shipping container made of honeycomb sandwich panels. Blekinge Inst. Technol. 2018; 7: 859-864.

[23] Yang XJ, Lan QS, Zhong YN. Buckling analysis and experiment of fiber-paper honeycomb sandwich structure composites. Adv. Mater. Res. 2011; 314: 566-570.

[24] Adapa SS, Jaggavarapu J, Vedangi V. Structural analysis of copper honeycomb structures. J. Adv. Eng. Technol. 2015; 8: 950.

[25] Rao KK, Rao KJ, Sarwade AG, Chandra MS. Strength analysis on honeycomb sandwich panels of different materials. Int. J. Eng. Res. Appl. 2012; 2: 365-374.

[26] Jangavali KA, Kamble DP. Finite element analysis and experimental evolution of honeycomb panel. Int. J. Sci. Res. 2016; 5: 1070-1073.

[27] Wang Z, Zhang J, Li Z, Shi C. On the crashworthiness of bio-inspired hexagonal prismatic tubes under axial compression. Int. J. Mech. Sci. 2020; 186: 105893.

[28] Alghamdi AAA. Collapsible impact energy absorbers: An overview. Thin. Walled Struct. 2001; 39: 189-213.

[29] Ha NS, Lu G. Thin-walled corrugated structures: A review of crashworthiness designs and energy absorption characteristics. Thin. Walled Struct. 2020; 157: 106995.

[30] Abramowicz W. Thin-walled structures as impact energy absorbers. Thin. Walled Struct. 2003; 41: 91-107.

[31] Fang J, Bao W, Ren F, Guan T, Xue G, Jiang J. Experimental study of hysteretic behavior of semi-rigid frame with a corrugated plate. J. Constr. Steel Res. 2020; 174: 106289.

[32] Clayton PM, Winkley TB, Berman JW, Lowes LN. Experimental investigation of self-centering steel plate shear walls. J. Struct. Eng. 2012; 7: 952-960.

[33] Emami F, Mofid M, Vafai A. Experimental study on cyclic behavior of trapezoidally corrugated steel shear walls. Eng. Struct. 2013; 48: 750-762.

[34] Qiu J, Zhao Q, Yu C, Li Z. Experimental studies on cyclic behavior of corrugated steel plate shear walls. J. Struct. Eng. 2018; 144: 04018200.

[35] He C, Qiu C, Zhang Z, Wei J, Zhang H, Tian N, Qin G. Microstructure and mechanical properties of 6061 al/az31 mg joints friction stir lap welded by a tool with variable-pitch thread pin. Metals 2021; 11: 34.

[36] Heinz A, Haszler A, Keidel C, Moldenhauer S, Benedictus R, Miller WS. Recent development in aluminium alloys for aerospace applications. Mater. Sci. Eng. A. 2000; 280: 102-107.

[37] Xue Y, Hu W, Hu X. Thermal Analysis of Textiles and Fibers, 2nd ed.; Elsevier: Amsterdam, Netherland, 2020.

[38] Brischetto S, Torre R. Exact 3D solutions and finite element 2D models for free vibration analysis of plates and cylinders. Curved. Layered. Struct. 2014; 1: 59-92.

[39] Soltani Z, Kordkheili SAH, Kress G. Experimental and numerical study of geometrically nonlinear behavior of corrugated laminated composite shells using a nonlinear layer-wise shell FE formulation. Eng. Struct. 2019; 184: 61-73.

[40] Arshid H, Khorasani M, Javid ZS, Dimitri R, Tornabene F. Quasi-3D hyperbolic shear deformation theory for the free vibration study of honeycomb microplates with graphene nanoplatelets-reinforced epoxy skins. Molecules. 2020; 25: 5085.

[41] Alaimo A, Orlando C, Valvano S. An alternative approach for modal analysis of stiffened thin-walled structures with advanced plate elements. Eur. J. Mech. A/Sol. 2019; 77: 103820.

[42] Venuti F. Influence of pattern anisotropy on the structural behaviour of free-edge single-layer gridshells. Curved. Layered. Struct. 2021; 8: 119-129.

[43] Kumar SK, Harursampath D, Carrera E, Cinefra M, Valvano S. Modal analysis of delaminated plates and shells using Carrera Unified Formulation − MITC9 shell element. Mech. Adv. Mat. Struct. 2018; 25: 681-697.

[44] Malikan M, Dimitri R, Tornabene F. Effect of sinusoidal corrugated geometries on the vibrational response of viscoelastic nanoplates. Appl. Sci. 2018; 8: 1432.

[45] Pagani A, Valvano S, Carrera E. Analysis of laminated composites and sandwich structures by variable-kinematic MITC9 plate elements. J. Sandw. Struct. Mat. 2018; 20: 4-41.

[46] Simitses G, Hodges D. Fundamentals of Structural Stability; Butterworth-Heinemann: Oxford, United Kingdom, 2006.

[47] Muttaqie T, Thang DQ, Prabowo AR, Cho SR, Sohn JM. Numerical studies of the failure modes of ring-stiffened cylinders under hydrostatic pressure. Struct. Eng. Mech. 2019; 70: 431-443.

[48] Jones RM. Buckling of Bars, Plates, and Shells; Bull Ridge Corporation: Virgina, United States of America, 2006.